Mechanics of Materials 160 (2021) 103898

Contents lists available at ScienceDirect

Mechanics of Materials

journal homepage: www.elsevier.com/locate/mecmat

Research paper

Spectral element formulation for damped transversely isotropic Micropolar-Cosserat layered composite panels

S.K. Singh [a], A. Banerjee [b,*], R.K. Varma [a], S. Adhikari [c]

[a] Department of Civil Engineering, Indian Institute of Technology Jammu, Jagti, Nagrota, NH-44, India
[b] Department of Civil Engineering, Indian Institute of Technology Delhi, Hauz Khas, 110016, India
[c] Zienkiewicz Centre for Computational Engineering, Swansea University, Swansea SA1 8EN, UK

ARTICLE INFO

Keywords:
Constitutive modelling
Transformation matrix
Size-dependent behavior
Micropolar-Cosserat laminate
Spectral element method
Eigenvalue problems
Internal damped response

ABSTRACT

The present paper aims to develop governing equation of motion for in-plane dynamics of Micropolar-Cosserat composite models with damping. Constitutive model of linear elastic damping system is formulated for an anisotropic domain fiber-reinforced composite panels (FRCP); undergoing large macro as well as micro geometric deformations. The air damping and Kelvin–Voigt strain linear rate damping have been considered into the governing equations of model, while mathematical modelling and simulation of composite panel is restricted to the free-vibration and in-plane static response. The composite panel has been modeled as a Micropolar-Cosserat continuum assuming second-order micro-length of the fiber deformation; by embedding an additional equation of kinematics through the micro-rotation degree of freedom in the classical continuum model. This account for the in-plane curvature bending effects of composite panels during the loss of ellipticity of the governing equations. A transformation matrix based on Rodrigues' rotational formula for transversely isotropic Micropolar-Cosserat lamina has been introduced; which reduces it to the well-known non-classical (classical and couple-stress) elastic formulation. The equivalent single layer (ESL) resultant stresses of FRCP in global coordinates is introduced to calculate in-plane damped and undamped response. The geometric and material linear elastic model for FRCP is derived using the spectral element method within state–space approach, and the corresponding plane-stress finite element model is validated with the undamped responses. Analytical response of damped composite panel is proposed based on available undamped simulation results.

1. Introduction

In the field of mechanical and structural engineering, vibrational analysis plays important role to characterize the dynamic behavior of composites (Capsoni et al., 2013). The influence of damping enhancement and dissipation mechanisms have been so far investigated; and successfully adopted in characterization and control of fiber reinforced composite panels (FRCP) vibration (Adhikari, 2000). The effects of internal and external dissipation sources have been conducted on vibrational characteristics and control of damping systems (Adhikari, 2005). Most of the damping models that have been proposed for composite materials stem from viscoelastic material models. In these cases, the major damping dissipation comes from the polymeric matrix. One of the simplest way to represent damping dissipation is the use of linear viscoelastic Kelvin–Voigt model (Crane and Gillespie Jr, 1989; Chandra et al., 1999). The main advantage of the Kelvin–Voigt model is the requirement of less number of parameters to characterize the viscoelastic behavior of the material. This model is simple however, it fails to fully represent the physics underlying the mechanisms of energy dissipation. In view of that, it is important to accurately determine the vibrational characteristics of the damping model (Torvik, 2010; De Silva, 2007). Various studies have proposed the use of viscoelastic material (with respect to fiber–matrix) to induce higher damping dissipation. By increasing the matrix volume fraction, the damping dissipation will increase at the expense of stiffness and strength (Treviso et al., 2015; Kaliske and Rothert, 1995). The sandwich structures are emerging as noise and vibration control solution for lightweight structures (Sodano et al., 2004; Treviso et al., 2015). The damping can also be tuned by properly choosing composites constitutive parameters such as fiber aspect ratio, stacking sequence, and constituents properties (Chandra et al., 1999; Adams and Maheri, 2003). The present research of FRCP is limited to the analytical description of the dynamics of a damped composite structure.

* Corresponding author.
E-mail addresses: 2018rce0002@iitjammu.ac.in (S.K. Singh), abanerjee@iitd.ac.in (A. Banerjee), rajendra.varma@iitjammu.ac.in (R.K. Varma), S.Adhikari@swansea.ac.uk (S. Adhikari).

https://doi.org/10.1016/j.mechmat.2021.103898
Received 6 March 2021; Received in revised form 25 April 2021; Accepted 26 April 2021
Available online 24 June 2021

Table of symbols

The symbols and descriptions for panel used in the paper are as follows:

L	Length
W	Width
T	Thickness
A	Cross-section area
I	Second moment of area
$\rho_f,\ \rho_m$	Density of fiber and matrix
$\nu_f,\ \nu_m$	Poisson ratio of fiber and matrix
$E_f,\ E_m$	Young modulus of fiber and matrix
$G_f,\ G_m$	Shear modulus of fiber and matrix
$V_f,\ V_m$	Volume if fiber and matrix
$D_l,\ D_g$	Local and global constitutive matrices
l	Characteristics length
u_x	Longitudinal deflection
u_y	Transverse deflection
ϕ	Rotation of cross-section
ψ_z	Rigid micro-rotation
ψ	Independent micro-rotation
ϵ_x, ϵ_y	Normal strains
$\epsilon_{xy}, \epsilon_{yx}$	Transverse strains
γ_s	Symmetric shear strain
γ_a	Asymmetric shear strain
K_{xz}, K_{yz}	Plane-stress curvatures
σ_x, σ_y	Normal stresses
τ_{xy}, τ_{yx}	Shear stresses
m_{xz}, m_{yz}	Curvature moments
M_x	Moment force
Q_{xy}, Q_{yx}	Shear Force
P_{xz}	Curvature force
ζ	Eigenvector
Ω	Eigenvalue
ω	Forcing frequency
ω_n	Natural frequency
SDC	Damping coefficient of shear stress
BDC	Damping coefficient of bending stress

The application of FRCP in the field of engineering (e.g. construction, aerospace, marine, automobile, etc.) has significantly increased during the past decade (Isanaka et al., 2020) because of their tailorable properties like high specific strength and stiffness. Moreover, the viscoelastic character of composites (fiber and/or matrix) render them suitable for the high performance. The viscoelastic composite layer undergoes a periodic shear deformation which dissipates energy (Benayoune et al., 2008; Faggiani and Falzon, 2010; Gay, 2014; Chandra et al., 1999; Treviso et al., 2015). In general, composites pertaining to transversely isotropic fibers are surrounded by an isotropic polymer based matrix (Hasanyan and Waas, 2018a; Sharma et al., 2020). The interaction of these constituents exhibit complex mechanical behavior at macro and nano-scale (Hasanyan and Waas, 2018b; Roque et al., 2013; Kundalwal and Ray, 2012). The analysis of these composites have often relied on modeling them as equivalent material; by explicitly considering fiber and matrix constituents of the composite using the micromechanics of lamina (Kyriakides et al., 1995; Seidel and Lagoudas, 2006). The Kelvin–Voigt principle state that the linear elastostatic analysis can be converted into the dynamic linear viscoelastic one; by replacing static stresses and strains with analogous dynamic stresses and strains, respectively. This is a suitable method for micromechanical models to predict damping in aligned fiber-reinforced composites (Hashin, 1970; Suarez et al., 1986). The primary and secondary structural components of composite call for a deeper understanding of their static and dynamic characteristics. The use of static stiffness for the prediction of natural frequencies is acceptable; by assuming negligible damping dissipative factor for fiber–matrix material (Chandra et al., 1999; Treviso et al., 2015). In the micromechanics approach, the stiffness of the matrix orientation (bond matrix) along the direction perpendicular to the fiber orientation (fiber bonds) is accommodated to the elastic modulus of the lamina in the same direction (Yerramalli and Waas, 2004; Diana and Casolo, 2019; Hassanzadeh-Aghdam et al., 2018). The effective stresses of fiber and matrix are predominantly transmitted through the fibers because of the high stiffness and strength in comparison to the properties of the matrix material (Hyer and White, 2009). However, the load-carrying capacity of fibers is severely affected by the stiffness of the surrounding matrix phase. Normal stresses are transmitted by the fibres only; however, the transverse shear stresses are transmitted through matrix and fibers both (Matzenmiller et al., 1995). The damping dissipation of unidirectional lamina is found to have a maximum value at approximately 35° in flexure and at 45° in torsion. The peak capacity for flexure and torsion both appear in the angle-ply between 40° and 50°, and in case of cross-ply it depends on cross-ply ratio that defines the relative number of 0° and 90° plies. Among all the orientations, square diagonal (angle-ply of 45°) packing of fibers provided the best damping in cantilever configuration (Adams and Maheri, 1994, 2003; Chandra et al., 1999; Treviso et al., 2015).

Most of the research on damping of micro-structure in composite is limited to 2-D state of stress. The micro-structure of composite give rise to high stiffness combined with high viscoelastic loss. For mathematical modeling, the individual lamina is considered to be orthotropic or transversely isotropic, however assembly of lamina lies in the anisotropic domain through out the thickness. Further, a large difference in the elastic properties of constituents fiber and matrix lead to a high ratio of in-plane Young's modulus to transverse shear modulus of lamina (Lakes, 2002; Maity et al., 2020; Treviso et al., 2015; Chandra et al., 1999; Hasanyan and Waas, 2018b). The classical laminate theory which neglects the effect of micro-structure, is inadequate for analysis of multi layer composite. Thus for the reliable analysis more accurate theories like first order shear deformation theories and refined higher order theories have been used especially in thick laminates (Chandra et al., 1999; Treviso et al., 2015; Adams and Maheri, 2003). A Micropolar-Cosserat continuum is proposed to capture the curvature of edges, and study the response of FRCP at micro and nano-scale (Chang and Ma, 1991; Sadeghpour et al., 2020). This computation has been geared towards the modeling of composites by assuming as an ESL continuum concept (Alshibli et al., 2006; Wanji et al., 2012). So, the two-dimensional Micropolar-Cosserat composite plate and shell can be reduced into one-dimensional by treating them as ESL of composite structures (Sargsyan and Sargsyan, 2016; Karttunen et al., 2018). This assumption leads to the development of shear deformation theory so that the stiffness properties inside the studied ESL material can be assumed to be constant (Romanoff et al., 2007; Sargsyan, 2012; Huang et al., 2000). The localization of constant width of shear stiffness (or shear band) has been achieved by introducing the independent micro-rotation of small scale particles of solids (Anand and Gu, 2000; Ramezani et al., 2009). The resulting phenomenon predict the loss of ellipticity of the governing partial differential equations of FRCP (Hasanyan and Waas, 2018b). The asymmetric curvature of edge appears due to unbalanced orientation [45°/0°/45°] of lamina of FRCP (Davis, 2014). The shape of the edge is saddle due to positive Poisson ratio (Gupta et al., 2020).

The limitation of the classical and non-classical continuum except Micropolar-Cosserat theory is that the constitutive models are local due to the absence of the skew-symmetric part of the shear stress at the energy density and do not possess characteristics length (Ghugal and Shimpi, 2001; Wanji et al., 2012; Asghari et al., 2011). This

leads to excessive mesh dependency due to the ill-posedness of the problem at the onset of localization (Roque et al., 2013). Micropolar-Cosserat continuum introduces characteristics length into constitutive equations, which increases the order of the differential in the governing equations, which in-turn prevents the ill-posedness associated with the localization (Needleman, 1988). In this theory, the main assumption is that each point of the continuum can rotate independently (Ramezani et al., 2009; Rahaman et al., 2015; Bardet, 1994). Using this main assumption, the kinematic formulation yields the higher-order stresses and strains, such as curvature strains and couple stresses (Carrera and Zozulya, 2020a,b; Zozulya, 2018). Their presence results in asymmetric shear stresses and strains (Karttunen et al., 2018). The modeling of FRCP using Micropolar-Cosserat continuum has ability to quantify the local fiber rotation, curvature, bending and twisting moments at the micro-scale (Hasanyan and Waas, 2018b,a). Some of the notable works in this area include the study of fiber by considering the finite Micropolar-Cosserat continuum. This helps to avoid the issues presented with the geometrically and materially exact equations under the assumption of linear curvature strains (Fleck and Shu, 1995; Hasanyan and Waas, 2018b). In addition, a continuum model for fiber-reinforced composites with fiber bending and twisting effects were discussed by Steigmann (2015). In the present paper, a 1-D Micropolar-Cosserat FRCP based on the linear law of variation of displacement has been considered. Spectral element formulation within state-space approach is implemented for the evaluation of in-plane damped and undamped transversely isotropic layered composite panels (Ramezani et al., 2009; Banerjee, 2020; Dion and Commault, 1993).

2. Constitutive modeling of a Micropolar-Cosserat undamped lamina

The global constitutive behavior of the Micropolar-Cosserat composite panel is derived using the Rodrigues' rotational based formula of transfer matrix for transversely isotropic lamina (Hasanyan and Waas, 2018a,b). The constitutive model of the unidirectional-lamina comprises of following assumptions:

1. Plane-stress condition is considered as the theoretical basis for modelling the constitutive behavior of each lamina (Sigmund, 1995; Ongaro et al., 2018).
2. The rule of mixture is used to calculate the elastic moduli of the lamina from the properties of fiber and matrix in proportion to the volume ratio (Oda et al., 1982).
3. The stress–strain response of laminae vary non-linearly. However, linear elasticity in stress–strain space is assumed to hold, if the damage state does not change (Matzenmiller et al., 1995).
4. The transversely isotropic nature of the lamina is considered as homogenized continuum throughout the modelling process (Federico and Grillo, 2012; Hasanyan and Waas, 2018b).
5. The orientation of stresses are in tangential and normal to the fiber direction, and the symmetry of the lamina remains the same for all states of damage (Matzenmiller and Sackman, 1994; Sevostianov et al., 2018).

Three different set of equations are needed to characterize the free vibration of a composite panel (De Borst, 1991), namely

1. The equilibrium equation
$$\left[\nabla^T\right]\{\sigma\} + \rho\{g\} = 0, \tag{1}$$
2. Kinematics equation
$$\{\epsilon\} = [\nabla]\{U\}, \tag{2}$$
3. Constitutive equation
$$\{\sigma\} = [D]\{\epsilon\}, \tag{3}$$

where σ = stress vector, ρ = density, g = gravity vector, U = displacement vector, ϵ = strain vector, D = constitutive matrix and ∇ = Laplace operator. A 2-D classical continuum plane-stress condition for stress, strain and displacement are

$$\sigma = [\sigma_x\ \sigma_y\ \tau_{xy}]^T, \tag{4}$$

$$\epsilon = [\epsilon_x\ \epsilon_y\ \epsilon_{xy}]^T, \tag{5}$$

$$U = [u_x\ u_y]^T, \tag{6}$$

and the ∇ matrix attains the following format

$$\nabla^T = \begin{bmatrix} \frac{\partial}{\partial x} & 0 & \frac{\partial}{\partial y} \\ 0 & \frac{\partial}{\partial y} & \frac{\partial}{\partial x} \end{bmatrix}, \tag{7}$$

respectively. The constitutive matrix D for the lamina into the local directions is identical with the elastic stiffness of anisotropic material (Nettles, 1994; Lekhnitskii and Dill, 1964)

$$\begin{Bmatrix} \sigma_1^e \\ \sigma_2^e \\ \tau_{12}^e \end{Bmatrix} = \underbrace{\begin{bmatrix} D_{1111} & D_{1122} & 0 \\ D_{1122} & D_{2222} & 0 \\ 0 & 0 & 2D_{1212} \end{bmatrix}}_{D} \begin{Bmatrix} \epsilon_1^e \\ \epsilon_2^e \\ \epsilon_{12}^e \end{Bmatrix}. \tag{8}$$

The salient characteristic of the Micropolar-Cosserat continuum is the introduction of an extra independent micro-rotational degrees of freedom to the translational degrees of freedom of classical continuum (De Borst and Sluys, 1991; De Borst, 1991). So, for a 2-D Micropolar-Cosserat continuum the normal and relatives asymmetric strain (Singh et al., 2021) components are

$$\epsilon_x = \frac{\partial u_x}{\partial x} \text{ and } \epsilon_y = \frac{\partial u_y}{\partial y}, \tag{9}$$

$$\epsilon_{xy} = \left(\frac{\partial u_x}{\partial y} - \psi\right) = (\phi - \psi) \text{ and } \epsilon_{yx} = \left(\frac{\partial u_y}{\partial x} + \psi\right) = \left(u_y' + \psi\right). \tag{10}$$

The symmetric and skew-symmetric shear strains are

$$\gamma_s = \epsilon_{xy} + \epsilon_{yx}, \text{ and } \gamma_a = \epsilon_{yx} - \epsilon_{xy}. \tag{11}$$

Where, ψ is the independent micro-rotation of structure around the z-axis. The micro-curvature strains due to in-plane bending (Ramezani et al., 2009; Asghari et al., 2011) are introduced which do not appear in the classical continuum

$$K_{xz} = \frac{\partial \psi}{\partial x} \text{ and } K_{yz} = \frac{\partial \psi}{\partial y}. \tag{12}$$

The formulation of displacement vector (De Borst and Sluys, 1991) is defined as

$$U = [u_x\ u_y\ \psi]^T. \tag{13}$$

Similarly, the conjugate stress and couple stress vector

$$\sigma = \left[\sigma_x\ \sigma_y\ \tau_{xy}\ \tau_{yx}\ m_{xz}\ m_{yz}\right]^T, \tag{14}$$

and strain vector

$$\epsilon = \left[\epsilon_x\ \epsilon_y\ \epsilon_{xy}\ \epsilon_{yx}\ K_{xz}\ K_{yz}\right]^T, \tag{15}$$

can be defined from the other research article (Singh et al., 2021; De Borst and Sluys, 1991; De Borst, 1991). Then, the equilibrium conditions (1) and the kinematic relations (2) are still satisfied provided that the Laplace operator is further redefined as

$$\nabla^T = \begin{bmatrix} \frac{\partial}{\partial x} & 0 & 0 & \frac{\partial}{\partial y} & 0 & 0 \\ 0 & \frac{\partial}{\partial y} & \frac{\partial}{\partial x} & 0 & 0 & 0 \\ 0 & 0 & -1 & 1 & \frac{\partial}{\partial x} & \frac{\partial}{\partial y} \end{bmatrix}. \tag{16}$$

The elastic operator (or constitutive matrix) (Hasanyan and Waas, 2018a,b) for transversely isotropic (anisotropic domain) Micropolar-Cosserat lamina into the local directions is defined as

$$\begin{Bmatrix} \sigma_1^e \\ \sigma_2^e \\ \tau_{12}^e \\ \tau_{21}^e \\ m_{13}^e \\ m_{23}^e \end{Bmatrix} = \underbrace{\begin{bmatrix} D_{1111} & D_{1122} & 0 & 0 & 0 & 0 \\ D_{1122} & D_{2222} & 0 & 0 & 0 & 0 \\ 0 & 0 & D_{1212} & D_{1221} & 0 & 0 \\ 0 & 0 & D_{1221} & D_{2121} & 0 & 0 \\ 0 & 0 & 0 & 0 & D_{1313} & 0 \\ 0 & 0 & 0 & 0 & 0 & D_{2323} \end{bmatrix}}_{D} \begin{Bmatrix} \epsilon_1^e \\ \epsilon_2^e \\ \epsilon_{12}^e \\ \epsilon_{21}^e \\ K_{13}^e \\ K_{23}^e \end{Bmatrix}. \tag{17}$$

The constant value of constitutive matrix, D is given in Appendix A.2. In the above relation, there are eight independent material constants. In contrast to an isotropic micropolar constitutive relation, the bending modulus $(D_{1313} \neq D_{2323})$ are not equal. The additional feature is the inequality of the constants, which differentiates the shear response $(D_{1212} \neq D_{2121})$ of a fibrous volume element when loaded parallel versus transverse to the fiber direction (Hasanyan and Waas, 2018b,a).

3. Formulation of damped Micropolar-Cosserat lamina

A Kelvin–Voigt model is assumed to introduce dissipative forces arising from damping effects during the vibration and motion. The adopted method is most suitable for modeling the damping of a structure vibrating in the viscous air (Banks and Inman, 1991). The viscous model with damping dissipative force is directly proportional to the transverse velocity $\dot{u}_y(x,t)$ of the vibrating system, through the external linear viscous damping coefficient η_v. As the beam vibrates it must displace air causing the force, $\eta_v \dot{u}_y(x,t) = \xi_v u_y$ to be applied to the structural system (Banks and Inman, 1991). This theory of internal damping is analogous of strain rate damping, sometimes also called velocity damping; where additional shear, bending, and couple stresses are τ_{12}^d, σ_1^d and m_{13}^d, respectively. The damping stresses are linearly proportional to the strain velocity through damping coefficients s_d, b_d and c_d, respectively (Banks and Inman, 1991; Capsoni et al., 2013). The introduction of this concept into the undamped relationship for two-dimensional lamina gives

$$\begin{aligned} \sigma_1 = \sigma_1^e + \sigma_1^d &= \left\{ D_{1111}\epsilon_1^e + D_{1122}\epsilon_2^e + b_d\left(\dot{\epsilon}_1^e + \dot{\epsilon}_2^e\right)\right\} \\ &= \left(1 - i\omega\eta_b\right)\left\{ D_{1111}\epsilon_1^e + D_{1122}\epsilon_2^e \right\}, \end{aligned} \tag{18}$$

$$\begin{aligned} \sigma_2 = \sigma_2^e + \sigma_2^d &= \left\{ D_{1122}\epsilon_1^e + D_{2222}\epsilon_2^e + b_d\left(\dot{\epsilon}_1^e + \dot{\epsilon}_2^e\right)\right\} \\ &= \left(1 - i\omega\eta_b\right)\left\{ D_{1122}\epsilon_1^e + D_{2222}\epsilon_2^e \right\}, \end{aligned} \tag{19}$$

$$\begin{aligned} \tau_{12} = \tau_{12}^e + \tau_{12}^d &= \left\{ D_{1212}\epsilon_{12}^e + D_{1221}\epsilon_{21}^e + s_d\left(\dot{\epsilon}_{12}^e + \dot{\epsilon}_{21}^e\right)\right\} \\ &= \left(1 - i\omega\eta_s\right)\left\{ D_{1212}\epsilon_{12}^e + D_{1221}\epsilon_{21}^e \right\}, \end{aligned} \tag{20}$$

$$\begin{aligned} \tau_{21} = \tau_{21}^e + \tau_{21}^d &= \left\{ D_{1221}\epsilon_{12}^e + D_{2121}\epsilon_{21}^e + s_d\left(\dot{\epsilon}_{12}^e + \dot{\epsilon}_{21}^e\right)\right\} \\ &= \left(1 - i\omega\eta_s\right)\left\{ D_{1221}\epsilon_{12}^e + D_{2121}\epsilon_{21}^e \right\}, \end{aligned} \tag{21}$$

$$\begin{aligned} m_{13} = m_{13}^e + m_{13}^d &= D_{1313}K_{13}^e + c_d\dot{K}_{13}^e \\ &= \left(1 - i\omega\eta_c\right) D_{1313}K_{13}^e, \end{aligned} \tag{22}$$

$$\begin{aligned} m_{13} = m_{23}^e + m_{23}^d &= D_{2323}K_{23}^e + c_d\dot{K}_{23}^e \\ &= \left(1 - i\omega\eta_c\right) D_{2323}K_{23}^e, \end{aligned} \tag{23}$$

The Eqs. (18) to (23) for 2-D lamina can be written in matrix form as

$$\begin{Bmatrix} \sigma_1 \\ \sigma_2 \\ \tau_{12} \\ \tau_{21} \\ m_{13} \\ m_{23} \end{Bmatrix} = \left[D\right]_{6\times6} \begin{Bmatrix} \epsilon_1^e \\ \epsilon_2^e \\ \epsilon_{12}^e \\ \epsilon_{21}^e \\ K_{13}^e \\ K_{23}^e \end{Bmatrix}, \tag{24}$$

where $b_d = \eta_b f\left(D_{1111}, D_{1122}, D_{2222}\right)$, $s_d = \eta_s f\left(D_{1212}, D_{1221}, D_{2121}\right)$, $c_d = \eta_s f\left(D_{1313}, D_{2323}\right)$, $\xi_f = -i\omega\eta_v$, $\xi_\sigma = \left(1 - i\omega\eta_b\right)$, $\xi_\tau = \left(1 - i\omega\eta_s\right)$ $= \xi_m$, $D = \begin{bmatrix} \xi_\sigma D_{1111} & \xi_\sigma D_{1122} & 0 & 0 & 0 & 0 \\ \xi_\sigma D_{1122} & \xi_\sigma D_{2222} & 0 & 0 & 0 & 0 \\ 0 & 0 & \xi_\tau D_{1212} & \xi_\tau D_{1221} & 0 & 0 \\ 0 & 0 & \xi_\tau D_{1221} & \xi_\tau D_{2121} & 0 & 0 \\ 0 & 0 & 0 & 0 & \xi_m D_{1313} & 0 \\ 0 & 0 & 0 & 0 & 0 & \xi_m D_{2323} \end{bmatrix}$.

The asymmetric stress and strain tensors can be decomposed into their symmetric and skew-symmetric components as

$$\begin{aligned} \tau_{12} &= S_{12} - T_{12}, \\ \epsilon_{12}^e &= e_{12} - A_{12}, \end{aligned} \tag{25}$$

where,

$$\begin{aligned} S_{12} &= \frac{1}{2}\left(\tau_{12} + \tau_{21}\right) = S_{21}, \\ T_{12} &= \frac{1}{2}\left(\tau_{21} - \tau_{12}\right) = -T_{21}, \end{aligned} \tag{26}$$

S_{12} is the symmetric component and T_{12} is the skew-symmetric component of σ_{12}^e. Similarly, e_{12} and A_{12} are the symmetric and the skew symmetric components of ϵ_{12}^e, respectively. where

$$\begin{aligned} e_{12} &= \frac{1}{2}\left(\epsilon_{12}^e + \epsilon_{21}^e\right) = e_{21}, \\ A_{12} &= \frac{1}{2}\left(\epsilon_{21}^e - \epsilon_{12}^e\right) = -A_{21}. \end{aligned} \tag{27}$$

The constitutive relationship (17) based on above decomposition relation (25), (26) and (27) of Micropolar-Cosserat lamina is

$$\begin{Bmatrix} S_1 \\ S_2 \\ S_{12} \\ T_{12} \\ m_{13} \\ m_{23} \end{Bmatrix} = \underbrace{\begin{bmatrix} \xi_\sigma C_{11} & \xi_\sigma C_{12} & 0 & 0 & 0 & 0 \\ \xi_\sigma C_{12} & \xi_\sigma C_{22} & 0 & 0 & 0 & 0 \\ 0 & 0 & \xi_\tau C_{33} & \xi_\tau C_{34} & 0 & 0 \\ 0 & 0 & \xi_\tau C_{34} & \xi_\tau C_{44} & 0 & 0 \\ 0 & 0 & 0 & 0 & \xi_m C_{55} & 0 \\ 0 & 0 & 0 & 0 & 0 & \xi_m C_{66} \end{bmatrix}}_{D_l} \begin{Bmatrix} e_1 \\ e_2 \\ 2e_{12} \\ 2A_{12} \\ K_{13} \\ K_{23} \end{Bmatrix}, \tag{28}$$

It can be further written for the 1-D damped transversely isotropic lamina as

$$\begin{Bmatrix} S_1 \\ S_{12} \\ T_{12} \\ m_{13} \end{Bmatrix} = \underbrace{\begin{bmatrix} \xi_\sigma C_{11} & 0 & 0 & 0 \\ 0 & \xi_\tau C_{33} & \xi_\tau C_{34} & 0 \\ 0 & \xi_\tau C_{34} & \xi_\tau C_{44} & 0 \\ 0 & 0 & 0 & \xi_m C_{55} \end{bmatrix}}_{D_l} \begin{Bmatrix} e_1 \\ 2e_{12} \\ 2A_{12} \\ K_{13} \end{Bmatrix}, \tag{29}$$

The transformation of lamina stress and strain from local to global axis can be done using the matrix (Hasanyan and Waas, 2018b), described as Fig. 1.

$$\left[T\right]_{4\times4} = \begin{bmatrix} c^2 & cs & 0 & 0 \\ -2cs & \left(c^2 - s^2\right) & 0 & 0 \\ 0 & 0 & 1 & 0 \\ 0 & 0 & 0 & c \end{bmatrix}, \tag{30}$$

where c and s represents $\cos\theta$ and $\sin\theta$, respectively. Hence, the lamina stress–strain relationship in the global directions are derived as

$$\begin{Bmatrix} \sigma_x \\ S_{xy} \\ T_{xy} \\ m_{xz} \end{Bmatrix} = \underbrace{\left[T\right]^{-1}\left[D_l\right]\left[T\right]}_{D_g} \begin{Bmatrix} \epsilon_x \\ 2e_{xy} \\ 2A_{xy} \\ K_{xz} \end{Bmatrix}. \tag{31}$$

The arrangement of global constitutive matrix is as follows

$$\left[D_g\right]_{4\times4} = \begin{bmatrix} A_{1111_\xi} & A_{1112_\xi} & A_{1121_\xi} & 0 \\ A_{1211_\xi} & A_{1212_\xi} & A_{1221_\xi} & 0 \\ A_{2111_\xi} & A_{2112_\xi} & A_{2121_\xi} & 0 \\ 0 & 0 & 0 & D_{11_\xi} \end{bmatrix}, \tag{32}$$

From Eqs. (11), (31) and (32) it can be written

$$\begin{Bmatrix} \sigma_x \\ S_{xy} \\ T_{xy} \\ m_{xz} \end{Bmatrix} = \begin{bmatrix} A_{1111_\xi} & A_{1112_\xi} & A_{1121_\xi} & 0 \\ A_{1211_\xi} & A_{1212_\xi} & A_{1221_\xi} & 0 \\ A_{2111_\xi} & A_{2112_\xi} & A_{2121_\xi} & 0 \\ 0 & 0 & 0 & D_{11_\xi} \end{bmatrix} \begin{Bmatrix} \epsilon_x \\ \gamma_s \\ \gamma_a \\ K_{xz} \end{Bmatrix}. \tag{33}$$

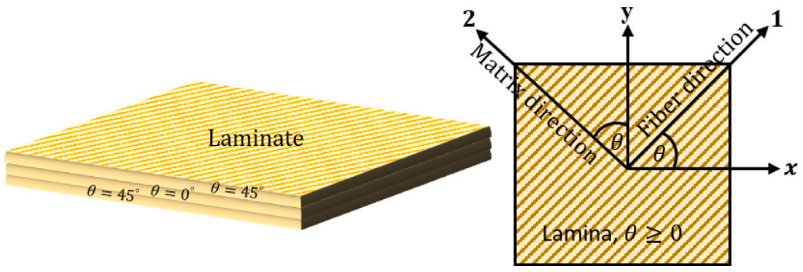

Fig. 1. Orientation of the fiber–matrix and stress–strain transformation of the unidirectional lamina.

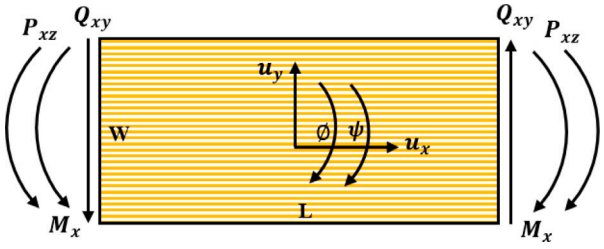

Fig. 2. Positive direction stress resultants of ne dimensional Micropolar-Cosserat panel with macro translation and rigid rotation of micro-structure.

The Eq. (33) gives symmetric and skew-symmetric shear-stresses as

$$S_{xy} = A_{1211_\xi}\epsilon_x + A_{1212_\xi}\gamma_s + A_{1221_\xi}\gamma_a,$$
$$T_{xy} = A_{2111_\xi}\epsilon_x + A_{2112_\xi}\gamma_s + A_{2121_\xi}\gamma_a. \tag{34}$$

So, asymmetric shear-stresses are

$$\tau_{xy} = S_{xy} - T_{xy} = \left\{\left(A_{1211_\xi} - A_{2111_\xi}\right)\epsilon_x + \left(A_{1212_\xi} - A_{2112_\xi}\right)\gamma_s + \left(A_{1221_\xi} - A_{2121_\xi}\right)\gamma_a\right\},$$
$$\tau_{yx} = S_{xy} + T_{xy} = \left\{\left(A_{1211_\xi} + A_{2111_\xi}\right)\epsilon_x + \left(A_{1212_\xi} + A_{2112_\xi}\right)\gamma_s + \left(A_{1221_\xi} + A_{2121_\xi}\right)\gamma_a\right\}. \tag{35}$$

The constant value global constitutive matrix of damped system is described in Appendix A.3.1. These asymmetric shear stresses are responsible for curvature moment/force of composite panel. On setting $\tau_{xy} = \tau_{yx}$, it will convert into the Timoshenko theory.

4. Balanced and governing equations of motion

Let us consider the stress and displacement field which do not vary across the width. The elastic constants are functions of x-coordinate. The stress–strain and couple stress components are independent from out of plane direction signifying that plane-stress element can be considered. The load is applied so that, no torsion occurs in the beam (Karttunen et al., 2018; Ramezani et al., 2009). The governing equations are considered together with boundary conditions on traction free faces ($\sigma_y = \tau_{yx} = K_{yz} = 0$, at ± y) (see Fig. 2).

4.1. Balanced equations of motion for the FRCP

A harmonic distributed external load, $f(t) = qe^{iwt}$, deals with the steady-state dynamic response of the system; however a time-independent function has been introduced to simplify the solution. The time-dependent balanced equations for 1-D Micropolar-Cosserat ESL composite panel are expressed as

$$\frac{\partial M_x}{\partial x} - Q_{yx} - \rho\frac{\partial^2 U_x}{\partial t^2} = 0, \tag{36}$$

$$\frac{\partial Q_{xy}}{\partial x} + \eta_v\frac{\partial u_y}{\partial t} - \rho A\frac{\partial^2 u_y}{\partial t^2} = f(t), \tag{37}$$

$$\frac{\partial P_{xz}}{\partial x} + \left(Q_{yx} - Q_{xy}\right) - \rho AJ\frac{\partial^2 \psi_z}{\partial t^2} = 0, \tag{38}$$

where $U_x = \int_A u_x y dA$, A = cross-section area, I = moment of inertia, and J = micro-inertia of panel (De Borst and Sluys, 1991). The stress resultants to reduce the 2-D equilibrium equations into 1-D balanced equations are as follows

$$M_x = \int_A N_x y dA,\ Q_{xy} = \int_A T_{xy} dA,\ Q_{yx} = \int_A T_{yx} dA \text{ and } P_{xz} = \int_A M_{xz} dA. \tag{39}$$

From the anisotropic stress–strain relationship Eqs. (33), (35) and stress resultants Eq. (39), following can be expressed for composite panel

$$N_x = \sum_{i=1}^{k}\sigma_x$$
$$M_x = \sum_{i=1}^{k} A_{1111_{\xi i}} I_i \phi' \tag{40}$$
$$T_{xy} = \sum_{i=1}^{k}\tau_{xy},$$
$$Q_{xy} = \sum_{i=1}^{k}\left[\left(B_{11_{\xi i}} + B_{12_{\xi i}}\right)A_i u_y' + \left(B_{11_{\xi i}} - B_{12_{\xi i}}\right)A_i\phi + 2B_{12_{\xi i}}A_i\psi\right]. \tag{41}$$
$$T_{yx} = \sum_{i=1}^{k}\tau_{yx},$$
$$Q_{yx} = \sum_{i=1}^{k}\left[\left(B_{21_{\xi i}} + B_{22_{\xi i}}\right)A_i u_y' + \left(B_{21_{\xi i}} - B_{22_{\xi i}}\right)A_i\phi + 2B_{22_{\xi i}}A_i\psi\right]. \tag{42}$$
$$M_{xz} = \sum_{i=1}^{k} m_{xz},$$
$$P_{xz} = \sum_{i=1}^{k} D_{11_{\xi i}}A_i\psi'. \tag{43}$$

P_{xz} represents the curvature force due to couple stresses on the basis of constitutive localization (at energy density level) (Ramezani et al., 2009; Karttunen et al., 2018). The stiffness parameter of damped ESL of panel is given in Appendix A.4.1.

4.2. Governing equations of motion for the FRCP

4.2.1. Dynamic model of composite

- Damped system: The time-independent governing equations of motion for 1-D Micropolar-Cosserat panel are derived by substituting the value of stress and force resultant (40) to (43) into balance equations of motion (36) to (38) are as follows

$$\sum_{i=1}^{k}\left[A_i\left\{\left(B_{11_{\xi i}} + B_{12_{\xi i}}\right)u_y'' + \left(B_{11_{\xi i}} - B_{12_{\xi i}}\right)\phi' + \cdots\right.\right.$$

$$\cdots + 2B_{12_{\xi i}}\psi' + \left(\rho_i\omega^2 + \xi_f\right)u_y\Big\}\Big] = q, \tag{44}$$

$$\sum_{i=1}^{k}\Big[A_{1111_{\xi i}}I_i\phi'' - \left(B_{21_{\xi i}} + B_{22_{\xi i}}\right)A_i u_y' + \cdots$$
$$\cdots - \left\{\left(B_{21_{\xi i}} - B_{22_{\xi i}}\right)A_i - \rho_i I_i\omega^2\right\}\phi - 2B_{22_{\xi i}}A_i\psi\Big] = 0, \tag{45}$$

$$\sum_{i=1}^{k}\Big[A_i\Big\{D_{11_{\xi i}}\psi'' + \left(E_{21_{\xi i}} - E_{11_{\xi i}}\right)u_y' + \cdots$$
$$\cdots + \left(E_{22_{\xi i}} - E_{12_{\xi i}}\right)\phi + \left(2B_{22_{\xi i}} - 2B_{12_{\xi i}} + \rho_i J_i\omega^2\right)\psi\Big\}\Big] = 0. \tag{46}$$

- Undamped system: If $\xi_\sigma = \xi_\tau = \xi_m = 1$ and $\xi_f = 0$, then damped system will be converted into undamped equation

$$\sum_{i=1}^{k}\Big[A_i\Big\{\left(B_{11_i} + B_{12_i}\right)u_y'' + \left(B_{11_i} - B_{12_i}\right)\phi' + 2B_{12_i}\psi' + \rho_i\omega^2 u_y\Big\}\Big] = q, \tag{47}$$

$$\sum_{i=1}^{k}\Big[A_{1111_i}I_i\phi'' - \left(B_{21_i} + B_{22_i}\right)A_i u_y' + \cdots$$
$$\cdots - \left\{\left(B_{21_i} - B_{22_i}\right)A_i - \rho_i I_i\omega^2\right\}\phi - 2B_{22_i}A_i\psi\Big] = 0, \tag{48}$$

$$\sum_{i=1}^{k}\Big[A_i\Big\{D_{11_i}\psi'' + \left(E_{21_i} - E_{11_i}\right)u_y' + \cdots$$
$$\cdots + \left(E_{22_i} - E_{12_i}\right)\phi + \left(2B_{22_i} - 2B_{12_i} + \rho_i J_i\omega^2\right)\psi\Big\}\Big] = 0. \tag{49}$$

4.2.2. Static model of composite

On setting the forcing frequency equal to zero into the damped system of Eqs. (47) to (49), the derived equations are as follows

$$\sum_{i=1}^{k}\Big[A_i\Big\{\left(B_{11_i} + B_{12_i}\right)u_y'' + \left(B_{11_i} - B_{12_i}\right)\phi' + 2B_{12_i}\psi'\Big\}\Big] = 0, \tag{50}$$

$$\sum_{i=1}^{k}\Big[A_{1111_i}I_i\phi'' - \left(B_{21_i} + B_{22_i}\right)A_i u_y' - \left(B_{21_i} - B_{22_i}\right)A_i\phi - 2B_{22_i}A_i\psi\Big] = 0, \tag{51}$$

$$\sum_{i=1}^{k}\Big[A_i\Big\{D_{11_i}\psi'' + \left(E_{21_i} - E_{11_i}\right)u_y' + \cdots$$
$$\cdots + \left(E_{22_i} - E_{12_i}\right)\phi + 2\left(B_{22_i} - B_{12_i}\right)\psi\Big\}\Big] = 0. \tag{52}$$

5. Analysis of Micropolar-Cosserat composite panels

5.1. In-plane static response

The analysis of In-plane static system can be done via the substitution method (Karttunen et al., 2018). But state–space method (Ramezani et al., 2009) is preferred for decoupling the system of partial differential equation with in transfer matrix frame-work. The linear differential equation (50) to (52) of the system can be written as

$$\left\{X'\right\}_{6\times1} = \sum_{i=1}^{k}\left[Z_i\right]_{6\times6}\left\{X\right\}_{6\times1}, \tag{53}$$

where the value of X and Z_i are $\left\{u_y \quad \phi \quad \psi \quad u_y' \quad \phi' \quad \psi'\right\}^T$ and

$$\begin{bmatrix} 0 & 0 & 0 & 1 & 0 & 0 \\ 0 & 0 & 0 & 0 & 1 & 0 \\ 0 & 0 & 0 & 0 & 0 & 1 \\ 0 & 0 & 0 & 0 & -\dfrac{E_{12_i}}{E_{11_i}} & -\dfrac{2B_{12_i}}{E_{11_i}} \\ 0 & \dfrac{E_{22_i}A_i}{A_{1111_i}I_i} & \dfrac{2B_{22_i}A_i}{A_{1111_i}I_i} & \dfrac{E_{21_i}A_i}{A_{1111_i}I_i} & 0 & 0 \\ 0 & \dfrac{E_{12_i} - E_{22_i}}{D_{11_i}} & 2\dfrac{B_{12_i} - B_{22_i}}{D_{11_i}} & \dfrac{E_{11_i} - E_{21_i}}{D_{11_i}} & 0 & 0 \end{bmatrix},$$

respectively. Using Eq. (13), Eq. (53) can be represent as

$$\begin{Bmatrix} U' \\ U'' \end{Bmatrix}_{6\times1} = \sum_{i=1}^{k}\left[Z_i\right]_{6\times6}\begin{Bmatrix} U \\ U' \end{Bmatrix}_{6\times1}. \tag{54}$$

The solution of the static system of linear differential equations (O'neil, 2011; Ramana, 2006; Chau, 2017) can be summarized as

$$\begin{Bmatrix} U \\ U' \end{Bmatrix}_{6\times1} = \sum_{i=1}^{k}\underbrace{\left[\zeta_i e^{\Omega_i x}\right]}_{S_i(x)}\left\{C\right\}_{6\times1},$$

$$\begin{Bmatrix} U \\ U' \end{Bmatrix}_{6\times1} = \sum_{i=1}^{k}\left[S_i(x)\right]_{6\times6}\left\{C\right\}_{6\times1}. \tag{55}$$

Where, ζ_i and Ω_i are eigenvector and eigenvalue of $\left[Z_i\right]$, respectively. Using displacement and stress resultants, the state vector for FRCP can be represent

$$\left\{V\right\}_{6\times1} = \sum_{i=1}^{k}\left[R_i\right]_{6\times6}\begin{Bmatrix} U \\ U' \end{Bmatrix}, \tag{56}$$

where the value of V and R_i are $\left\{u_y \quad \phi \quad \psi \quad M_x \quad Q_{xy} \quad P_{xz}\right\}^T$ and

$$\begin{bmatrix} 1 & 0 & 0 & 0 & 0 & 0 \\ 0 & 1 & 0 & 0 & 0 & 0 \\ 0 & 0 & 1 & 0 & 0 & 0 \\ 0 & 0 & 0 & 0 & A_{1111_i}I_i & 0 \\ 0 & \left(B_{21_i} - B_{22_i}\right)A_i & 2B_{22_i}A_i & \left(B_{21_i} + B_{22_i}\right)A_i & 0 & 0 \\ 0 & 0 & 0 & 0 & 0 & D_{11_i}A_i \end{bmatrix},$$

respectively. From the Eqs. (55) and (56), the state vector is represented as

$$\left\{V(x)\right\}_{6\times1} = \sum_{i=1}^{k}\left[R_i\right]_{6\times6}\left[S_i(x)\right]_{6\times6}\left\{C\right\} \tag{57}$$

On substituting $x = 0$, and $x = L$ in Eqs. (57); the matrix relation between the state-vector and coefficient of two boundaries can be expressed as

$$\left\{C\right\}_{6\times1} = \sum_{i=1}^{k}\left[S_i(0)\right]_{6\times6}^{-1}\left[R_i\right]_{6\times6}^{-1}\left\{V(0)\right\}_{6\times1}, \tag{58}$$

and

$$\left\{C\right\}_{6\times1} = \sum_{i=1}^{k}\left[S_i(L)\right]_{6\times6}^{-1}\left[R_i\right]_{6\times6}^{-1}\left\{V(L)\right\}_{6\times1}. \tag{59}$$

From the coefficient of Eq. (58), the state vector for boundary values can be written as

$$\left\{V(L)\right\}_{6\times1} = \sum_{i=1}^{k}\underbrace{\left[R_i\right]_{6\times6}\left[S_i(L)\right]_{6\times6}\left[S_i(0)\right]_{6\times6}^{-1}\left[R_i\right]_{6\times6}^{-1}}_{T_{s_i}}\left\{V(0)\right\}_{6\times1}. \tag{60}$$

Let us assume, the transfer matrix of a static system as

$$\left[T_{s_i}\right]_{6\times6} = \sum_{i=1}^{k}\begin{bmatrix} T_{11_i} & T_{12_i} \\ T_{21_i} & T_{22_i} \end{bmatrix}_{6\times6}.$$

From the Eq. (60), it can written

$$\begin{Bmatrix} D_2 \\ F_2 \end{Bmatrix}_{6\times1} = \begin{bmatrix} T_{11_i} & T_{12_i} \\ T_{21_i} & T_{22_i} \end{bmatrix} \begin{Bmatrix} D_1 \\ F_1 \end{Bmatrix}_{6\times1}, \tag{61}$$

where $\{D_j\}^T = \begin{Bmatrix} u_{y_j} & \phi_j & \psi_j \end{Bmatrix}$, $\{F_j\}^T = \begin{Bmatrix} M_{x_j} & Q_{xy_j} & P_{xz_j} \end{Bmatrix}$ and j=1, 2. From the Eq. (61), the relationship between displacement, force, and transfer matrix is expressed as

$$\begin{Bmatrix} Q_{xy_1} \\ M_{x_1} \\ P_{xz_1} \end{Bmatrix} = \sum_{i=1}^{k} \left[T_{12_i}\right]_{3\times3}^{-1} \begin{Bmatrix} u_{y_2} \\ \phi_2 \\ \psi_2 \end{Bmatrix} - \sum_{i=1}^{k} \left[T_{12_i}\right]_{3\times3}^{-1} \left[T_{11_i}\right]_{3\times3} \begin{Bmatrix} u_{y_1} \\ \phi_1 \\ \psi_1 \end{Bmatrix}, \tag{62}$$

$$\begin{Bmatrix} Q_{xy_2} \\ M_{x_2} \\ P_{xz_2} \end{Bmatrix} = \sum_{i=1}^{k} \left[T_{21_i} - T_{22_i} T_{12_i}^{-1} T_{11_i}\right]_{3\times3} \begin{Bmatrix} u_{y_1} \\ \phi_1 \\ \psi_1 \end{Bmatrix} + \cdots \cdots + \sum_{i=1}^{k} \left[T_{22_i}\right]_{3\times3} \left[T_{12_i}\right]_{3\times3}^{-1} \begin{Bmatrix} u_{y_2} \\ \phi_2 \\ \psi_2 \end{Bmatrix}, \tag{63}$$

By assembling Eqs (62) and (63), the relation between damping force and displacement can be expressed as

$$\begin{Bmatrix} F_1 \\ F_2 \end{Bmatrix}_{6\times1} = \sum_{i=1}^{k} \begin{bmatrix} -T_{12_i}^{-1} T_{11_i} & T_{12_i}^{-1} \\ T_{21_i} - T_{22_i} T_{12_i}^{-1} T_{11_i} & T_{22_i} T_{12_i}^{-1} \end{bmatrix}_{6\times6} \begin{Bmatrix} D_1 \\ D_2 \end{Bmatrix}_{6\times1}. \tag{64}$$

The composite panel is solved as a 1-D cantilever elastic panel. Hence, for fixed end, $\{D_1\} = 0$ and for free end, $M_{x_2} = 0$ but $Q_{xy_2} \neq 0$ and $P_{xz_2} \neq 0$. It can be derived from Eqs. (62) and (63) as

$$\begin{Bmatrix} u_{y_2} \\ \phi_2 \\ \psi_2 \end{Bmatrix} = \sum_{i=1}^{k} \left[T_{12_i}\right]_{3\times3} \left[T_{22_i}\right]_{3\times3}^{-1} \begin{Bmatrix} 0 \\ Q_{xy_2} \\ P_{xz_2} \end{Bmatrix}, \tag{65}$$

where flexibility and stiffness matrix of cantilever panel are, $\left[F\right]_{3\times3} = \sum_{i=1}^{k} \left[T_{12_i}\right]_{3\times3} \left[T_{22_i}\right]_{3\times3}^{-1}$ and $\left[K_s\right]_{3\times3} = \left[F\right]_{3\times3}^{-1}$, respectively. The value of $\{D_2\}^T = \frac{1}{L}\left[F\right]_{3\times3}$, which helps to calculate the curvature moment, $P_{xz_2} = 2GK_{xz_2}l^2$. From the Eq. (59) and (65) the value of coefficient is derived as

$$\{C\}_{6\times1} = \sum_{i=1}^{k} \left[R_i\right]_{6\times3}^{-1} \left[S_i(L)\right]_{3\times3}^{-1} \left[T_{12}\right]_{3\times3} \left[T_{22}\right]_{3\times3}^{-1} \begin{Bmatrix} 0 \\ Q_{xy_2} \\ P_{xz_2} \end{Bmatrix}_{3\times1}, \tag{66}$$

The value of the Eq. (66) is used with Eq. (57) to find out macro and micro-displacements, yield stress and force resultants of cantilever FRCP. The finite element analysis (with the help of ABAQUS software) of plane-stress element to validate the in-plane static response is shown in Fig. 3. The volume and surface area of panel are LWT and $2(LW + LT + WT)$, respectively. The salient features of the finite element model are given as

1. Geometry: 3-D deformable shell planar.
2. Section: Homogeneous solid.
3. Mesh size: 0.025 m.
4. Mesh controls: Quad-dominated.
5. Element shape: Quad.
6. Element type: S4R.

S4R is 4-node general-purpose shell with reduced integration of hour-glass control to avoid the shear and membrane strain. This Converges to shear flexible theory for thick shells and classical theory for thin shells (Hibbitt et al., 1997).

5.2. Dynamic response of composite panel

The dynamic system of coupled Eqs. (44) to (46) have no classical representation. So, it is necessary to represent the coupled system as a two-scale matrix via sufficient and necessary decoupling conditions (Dion and Commault, 1993). The separation variable matrix of coupled equations is expressed as

$$\sum_{i=1}^{k} \left[M_{\xi i} U'' + D_{\xi i} U' + K_{\xi i} U\right] = 0,$$

$$\sum_{i=1}^{k} \left[U'' + M_{\xi i}^{-1} D_{\xi i} U' + M_{\xi i}^{-1} K_{\xi i} U\right] = 0, \tag{67}$$

where value of $M_{\xi i} = \begin{bmatrix} \left(B_{11_{\xi i}} + B_{12_{\xi i}}\right) A_i & 0 & 0 \\ 0 & A_{1111_{\xi i}} I_i & 0 \\ 0 & 0 & D_{11_{\xi i}} A_i \end{bmatrix}$, $D_{\xi i} = \begin{bmatrix} 0 & \left(B_{11_{\xi i}} - B_{12_{\xi i}}\right) A_i & 2B_{12_{\xi i}} A_i \\ -\left(B_{21_{\xi i}} + B_{22_{\xi i}}\right) A_i & 0 & 0 \\ \left(E_{21_{\xi i}} - E_{11_{\xi i}}\right) A_i & 0 & 0 \end{bmatrix}$, and the $K_{\xi i} = \begin{bmatrix} \rho_i A_i \omega^2 & 0 & 0 \\ 0 & \left\{\rho_i I_i \omega^2 - \left(B_{21_{\xi i}} - B_{22_{\xi i}}\right) A_i\right\} & -2B_{22_{\xi i}} A_i \\ 0 & \left(E_{22_{\xi i}} - E_{12_{\xi i}}\right) A_i & \left(2B_{22_{\xi i}} - 2B_{12_{\xi i}} + \rho_i J_i \omega^2\right) A_i \end{bmatrix}$, respectively. The generalized formulation of Eq. (67) via the graphical representation of state–space method are as follows

$$\underbrace{\begin{Bmatrix} U'' \\ U' \end{Bmatrix}_{6\times1}}_{X'} = \sum_{i=1}^{k} \underbrace{\begin{bmatrix} -M_{\xi i}^{-1} D_{\xi i} & -M_{\xi i}^{-1} K_{\xi i} \\ I_3 & 0 \end{bmatrix}_{6\times6}}_{Z_{\xi i}} \underbrace{\begin{Bmatrix} U' \\ U \end{Bmatrix}_{6\times1}}_{X},$$

$$\{X'\} = \sum_{i=1}^{k} \left[Z_{\xi i}\right] \{X\}. \tag{68}$$

The solution of the above dynamic system of linear differential equations (O'neil, 2011; Ramana, 2006; Chau, 2017) is summarized as

$$\begin{Bmatrix} U' \\ U \end{Bmatrix}_{6\times1} = \sum_{i=1}^{k} \underbrace{\left[\zeta_{\xi i} e^{\Omega_{\xi i} x}\right]}_{S_{\xi i}(x)} \{C\}_{6\times1},$$

$$\begin{Bmatrix} U' \\ U \end{Bmatrix}_{6\times1} = \sum_{i=1}^{k} \left[S_{\xi i}(x)\right]_{6\times6} \{C\}_{6\times1}. \tag{69}$$

Where, $\zeta_{\xi i}$ and $\Omega_{\xi i}$ are eigenvector and eigenvalue of $\left[Z_{\xi i}\right]$, respectively. The state vector (or V matrix) by using displacement u_y, ψ, ϕ and resultants force Eqs. (40) to (43) can be expressed as

$$\{V\}_{6\times1} = \sum_{i=1}^{k} \left[R_{\xi i}\right]_{6\times6} \begin{Bmatrix} U' \\ U \end{Bmatrix}_{6\times1}, \tag{70}$$

$$\begin{bmatrix} 0 & 0 & 0 & 1 & 0 & 0 \\ 0 & 0 & 0 & 0 & 1 & 0 \\ 0 & 0 & 0 & 0 & 0 & 1 \\ 0 & A_{1111_{\xi i}} I_i & 0 & 0 & 0 & 0 \\ (B_{21_{\xi i}} + B_{22_{\xi i}}) A_i & 0 & 0 & 0 & (B_{21_{\xi i}} - B_{22_{\xi i}}) A_i & 2B_{22_{\xi i}} A_i \\ 0 & 0 & D_{11_{\xi i}} A_i & 0 & 0 & 0 \end{bmatrix}$$

represents the value of $R_{\xi i}$. From the Eqs. (69) and (70), the relation between state vector and coefficient is expressed as

$$\{V(x)\}_{6\times1} = \sum_{i=1}^{k} \left[R_{\xi i}\right]_{6\times6} \left\{S_{\xi i}(x)\right\}_{6\times6} \{C\}_{6\times1}, \tag{71}$$

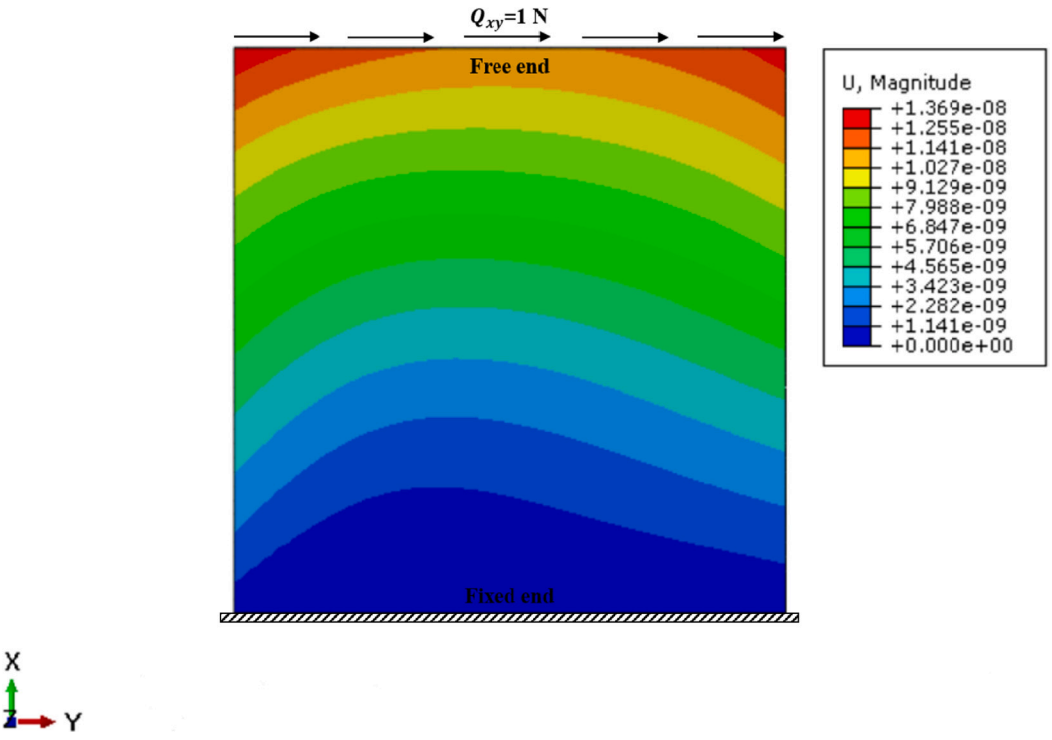

Fig. 3. In-plane static response, $U = \sqrt{u_x^2 + u_y^2}$ of undamped FRCP caused by the transverse shear traction; for dimension 1 m × 1 m × 0.15 m.

Using end conditions $x = 0$ and $x = L$, the relation between state vector $V(0)$ and $V(L)$ is expressed as

$$\{V(L)\}_{6\times1} = \sum_{i=1}^{k} \underbrace{[R_{\xi i}]_{6\times6} \{S_{\xi i}(L)\}_{6\times6} [S_{\xi i}(0)]^{-1}_{6\times6} \{R_{\xi i}\}^{-1}_{6\times6}}_{T_{\xi i}} \{V(0)\}_{6\times1}. \tag{72}$$

Let us assume, the transfer matrix of a dynamic system as

$$[T_{\xi i}]_{6\times6} = \sum_{i=1}^{k} \begin{bmatrix} T_{11_{\xi i}} & T_{12_{\xi i}} \\ T_{21_{\xi i}} & T_{22_{\xi i}} \end{bmatrix}_{6\times6},$$

So, Eq. (72) can be written as

$$\begin{Bmatrix} D_2 \\ F_2 \end{Bmatrix}_{6\times1} = \sum_{i=1}^{k} \begin{bmatrix} T_{11_{\xi i}} & T_{12_{\xi i}} \\ T_{21_{\xi i}} & T_{22_{\xi i}} \end{bmatrix}_{6\times6} \begin{Bmatrix} D_1 \\ F_1 \end{Bmatrix}_{6\times1}, \tag{73}$$

By using spectral element method, the Eq (73) can be described as

$$\{F_1\} = \sum_{i=1}^{k} \left[T_{12_{\xi i}}\right]^{-1}_{3\times3} \{D_2\} - \sum_{i=1}^{k} \left[T_{12_{\xi i}}\right]^{-1}_{3\times3} \left[T_{11_{\xi i}}\right]_{3\times3} \{D_1\}, \tag{74}$$

Similarly,

$$\{F_2\} = \sum_{i=1}^{k} \left[T_{21_{\xi i}} - T_{22_{\xi i}} T^{-1}_{12_{\xi i}} T_{11_{\xi i}}\right]_{3\times3} \{D_1\} + \cdots$$
$$\cdots + \sum_{i=1}^{k} \left[T_{22_{\xi i}}\right]_{3\times3} \left[T_{12_{\xi i}}\right]^{-1}_{3\times3} \{D_2\}, \tag{75}$$

By assembling Eqs. (74) and (75), we can get relation between force based damping and displacement

$$\begin{Bmatrix} F_1 \\ F_2 \end{Bmatrix}_{6\times1} = \sum_{i=1}^{k} \begin{bmatrix} -T^{-1}_{12_{\xi i}} T_{11_{\xi i}} & T^{-1}_{12_{\xi i}} \\ T_{21_{\xi i}} - T_{22_{\xi i}} T^{-1}_{12_{\xi i}} T_{11_{\xi i}} & T_{22_{\xi i}} T^{-1}_{12_{\xi i}} \end{bmatrix}_{6\times6} \begin{Bmatrix} D_1 \\ D_2 \end{Bmatrix}_{6\times1}. \tag{76}$$

where $\{D_j\}^T = \{u_{y_j} \quad \phi_j \quad \psi_j\}$, $\{F_j\}^T = \{M_{x_j} \quad Q_{xy_j} \quad P_{xz_j}\}$ and j=1, 2. For a cantilever panel, the relation between displacement and force is

$$\begin{Bmatrix} u_{y_2} \\ \phi_2 \\ \psi_2 \end{Bmatrix} = \sum_{i=1}^{k} \left[T_{12_{\xi i}}\right]_{3\times3} \left[T_{22_{\xi i}}\right]^{-1}_{3\times3} \begin{Bmatrix} 0 \\ Q_{xy_2} \\ P_{xz_2} \end{Bmatrix}, \tag{77}$$

The value of coefficient is

$$\{C\}_{6\times1} = \sum_{i=1}^{k} [R_{\xi i}]^{-1}_{6\times3} [S_{\xi i}(L)]^{-1}_{3\times3} \left[T_{12_{\xi i}}\right]_{3\times3} \left[T_{22_{\xi i}}\right]^{-1}_{3\times3} \begin{Bmatrix} 0 \\ Q_{xy_2} \\ P_{xz_2} \end{Bmatrix}_{3\times1}. \tag{78}$$

The analytical relation between stiffness parameter and damped frequency can be evaluated from the Eq. (76) for any type of boundary conditions.

5.3. Natural frequency of composite panel

The necessary and sufficient conditions to convert a damped system into an undamped one are; $\xi_\sigma = \xi_\tau = \xi_m = 1$ and $\xi_f = 0$. The undamped relation between state vector $V(0)$ and $V(L)$ for boundary conditions, $x = 0$ and $x = L$ is expressed as

$$\{V(L)\}_{6\times1} = \sum_{i=1}^{k} \underbrace{[R_i]_{6\times6} \{S_i(L)\}_{6\times6} [S_i(0)]^{-1}_{6\times6} \{R_i\}^{-1}_{6\times6}}_{T_{di}} \{V(0)\}_{6\times1}. \tag{79}$$

Let us assume, the transfer matrix of an undamped dynamic system as

$$[T_{di}]_{6\times6} = \sum_{i=1}^{k} \begin{bmatrix} T_{11_i} & T_{12_i} \\ T_{21_i} & T_{22_i} \end{bmatrix}_{6\times6},$$

Eq. (79) can be written as

$$\{V(L)\}_{6\times1} = \sum_{i=1}^{k} \begin{bmatrix} T_{11_i} & T_{12_i} \\ T_{21_i} & T_{22_i} \end{bmatrix}_{6\times6} \{V(0)\}_{6\times1}, \tag{80}$$

So within spectral element framework, new relation of static stiffness with force and displacement using state–space approach is

$$\begin{Bmatrix} F_1 \\ F_2 \end{Bmatrix}_{6\times1} = \sum_{i=1}^{k} \begin{bmatrix} -T_{12_i}^{-1}T_{11_i} & T_{12_i}^{-1} \\ T_{21_i} - T_{22_i}T_{12_i}^{-1}T_{11_i} & T_{22_i}T_{12_i}^{-1} \end{bmatrix}_{6\times6} \begin{Bmatrix} D_1 \\ D_2 \end{Bmatrix}_{6\times1}, \tag{81}$$

For the forcing frequencies (or ω); when the values of transfer matrix coefficient, $\left[T_{22_i}T_{12_i}^{-1}\right]_{3\times3}$ will be equal to zero; those values will be natural frequencies (or ω_n). The finite element analysis of Plane-stress element to validate the free-vibration response is shown in Fig. 4. The volume and surface area of panel are LWT and $2(LW + LT + WT)$, respectively. The salient features of finite element model for evaluating natural frequencies of the cantilever panel are given as

1. Geometry: 3-D deformable shell planar.
2. Section: Homogeneous solid.
3. Mesh size: 0.025 m.
4. Mesh controls: Quad-dominated
5. Element shape: Quad.
6. Element type: S4R.

6. Results discussion of anisotropic domain FRCP

Consider a composite cantilever panel with following geometric and material properties to compare the in-plane static and natural frequency response: Modulus of elasticity, $E_f = 72.40$ GPa and $E_m = 3.45$ GPa. Poisson ratio, $\nu_f = 0.22$ and $\nu_m = 0.35$. Mass density, $\rho_f = 2600\ \mathrm{kg/m^3}$ and $\rho_m = 1200\ \mathrm{kg/m^3}$. Volume fraction, $V_f = 0.70$ and $V_m = 0.30$. Length, $L = 1\ to\ 3$ m, Width, $W = 0.15\ to\ 2.75$ m, Thickness of lamina, $t_l = 0.05$ m and Thickness of laminate, $T = 0.15$ m. The effective elastic properties and orientation of composite lamina are described in the Table 1.

6.1. Displacement of composite panel

Micropolar-Cosserat analysis with respect to FE analysis for $1\ \mathrm{N/m^2}$ surface traction at free end with the varying dimensions are summarized in the sections given below:

- The lateral deflection and corresponding stiffness of cantilever panels are found directly from FE analysis. Typical graphs for comparative analysis of lateral deflection and stiffness are shown in Fig. 5.
- The rotation of cross-section is derived with the help of longitudinal and lateral deflections of a panel which are found from FE analysis. Typical sketch, formulation of macro and micro-rotation (Singh et al., 2021), and graphical comparison of rotation of cross-section is shown in Fig. 5. The rotation of cross-section about the neutral axis is expressed as

$$\phi = \left[-\frac{u_x}{y} + \frac{\sqrt{AB_x^2 + AB_y^2}}{y} \right], \tag{82}$$

  where, $AB_x = -\frac{W}{2}\sin\theta$, $AB_y = \frac{W}{2}(1-\cos\theta)$, $\theta = \frac{\partial u_y}{\partial x}$, and $y = \frac{W}{2}$.
- The relative rotation of micro-structure (Singh et al., 2021) based on the displacement field are shown in Fig. 5. The average rotations of micro-structure is

$$\psi = \frac{1}{2}\left(\phi - \frac{\partial u_y}{\partial x}\right) \tag{83}$$

  Using the Eq. (82) and (83), micro-rotation is based on lateral and longitudinal displacement as described by

$$\psi = \frac{1}{2}\left[-\frac{u_x}{y} + \frac{\sqrt{AB_x^2 + AB_y^2}}{y} - \frac{\partial u_y}{\partial x} \right] \tag{84}$$

The finite element solutions for in-plane static responses predicted by ABAQUS are in excellent agreement with Micropolar-Cosserat analytical solutions using the spectral element method within state-space framework. This theory provides curvature moment to capture the curvature of edges; and as the size of panel increases the corresponding best response comes out for in-plane undamped layered composite panel (Ramezani et al., 2009; Karttunen et al., 2018). The macro and micro-displacement of fiber–matrix composite into Micropolar-Cosserat framework is based on the second-order scale length parameters (Hasanyan and Waas, 2018b). The constitutive matrix (or energy density), and characteristics length (or strain softening) based curvature moment is the function of localization of mesh sensitivity of composite panel (Eaton et al., 1995). The localization associated with strain softening is neither necessary nor sufficient in setting the constant width of the shear band and energy dissipation during the time of computation (De Borst and Sluys, 1991; Needleman, 1988).

6.2. Natural frequency

The numerical value of $\sqrt{\frac{\rho L^2}{G_{12}}}$ has been multiplied with natural frequency and plotted against the reduced scale natural frequency for FRCP cantilever panel; and compared graph is shown in Fig. 5. The natural frequency response of Micropolar-Cosserat composite panel matches closely to numerical analysis of plane-stress element. Another important feature of the composite materials is the bond behavior; the matrix damage in laminated composites accounting for the inhomogeneous distinct properties of the fiber and matrix, i.e. the elastic constants, are continuous functions of the bond orientation in the principal axes (Daniel et al., 1994). So, macro-mechanics of composite laminates and corresponding stiffness of off-axis modulus changes continuously with respect to the delamination of fiber orientation in a unidirectional lamina (Diana and Casolo, 2019; Zhou et al., 2017; Mikata, 2019). The continuous change into the off-axis modulus leads to wave mode conversion (Munian et al., 2018). The propagation of waves having high frequencies or short wave lengths (Lan et al., 2014), in particular, when the wave length is of the same order of magnitude as the average dimension of the micro-elements, the intrinsic motion of the micro-elements with respect to the center of mass affects the outcome appreciably (Singh et al., 2018).

6.3. Damping response of the panel

The response of a FRCP for $1\ \mathrm{N/m^2}$ as a surface traction at free end with internal damping only, and with zero external damping are plotted in Fig. 6. In-plane static response and natural frequency of composite panel is matching with undamped response of Fig. 6. The macro and micro-displacement has been normalized with respect to its static value of damped response; where size of panel considered is 1 m × 1 m × 0.15 m. Macro and micro-displacement, as well as forcing frequency is gradually decreasing due to damping dissipation (Scerrato, 2014). The amplitude and phase angle of the response of a viscoelastic damped system at resonance is dependent on the damping coefficient of the system (Capsoni et al., 2013). In a viscoelastic damped system, resonance occurs when damped forcing frequency is equal to undamped natural frequency (Foley et al., 2008). So, for ratio of damped forcing frequency to undamped natural frequency much lesser than 1, resonance is very close to undamped natural frequency and hence the phase difference angle is, $-\pi/2$. Also, it is noteworthy that the phase before resonance is very close to zero and after resonance is, $-\pi$ (Luongo and Zulli, 2020). Similarly, the amplitude is very low expect near the resonant frequency. When the phase angle reaches close to zero degree, then the amplitude reaches close to 1, i.e. very less amplification is observed (Joris and Yin, 1992). So, to summarize, as damping increases in the system, both the phase angle and amplitude at resonance decreases. Also, the rate of

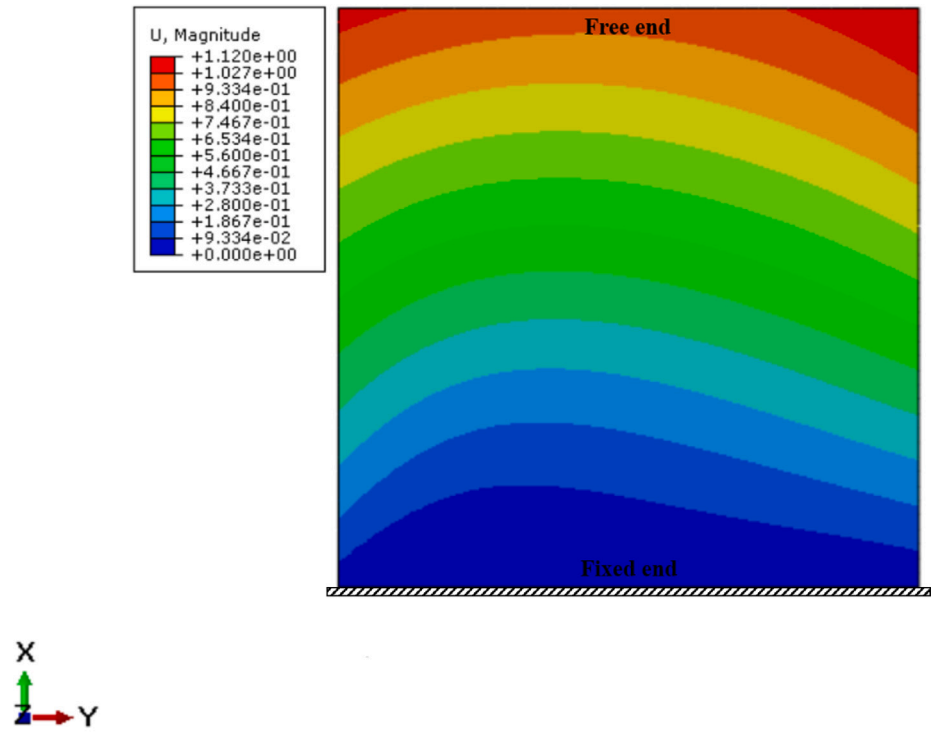

Fig. 4. FE undamped model based static stiffness for the natural frequency of first mode is 534.22 Hz; for dimension 1000 mm × 1000 mm × 150 mm.

Table 1

E_{11} (GPa)	$E_{22} = E_{33}$ (GPa)	$G_{12} = G_{13}$ (GPa)	G_{23} (GPa)	$\nu_{12} = \nu_{13}$	ν_{23}	ρ (kg/m^3)	θ (deg)
51.72	10.35	6.91	3.89	0.26	0.33	2180	45/0/45

Note: Relation between poisson ratio and young modulus is $\nu_{23} < \left\{1 - 2\nu_{13}^2\left(\frac{E_{11}}{E_{33}}\right)\right\}$.

change near the neighborhood decreases which means that the transition near the resonance is smoother (Baer et al., 1989). Phase response at resonance frequency for stiffness element, $[K_{33}]$ and $[K_{66}]$ of FRCP is changing from one phase to another phase. The phase propagation through the composite panel has negative and positive slope at the left and right side of the resonance frequency, respectively. So, the medium has a band-gap region of zero wave propagation at resonance, which results in constant phase across the medium (Aydin et al., 2004). In other words, the propagation of the wave is backward at the resonance which results in negative phase slope across the medium (Nguyen et al., 2018).

The individual behavior of diagonal stiffness element and corresponding phase angle are shown in Fig. 7 and Fig. 8, respectively. The diagonal stiffness elements have been normalized by the corresponding static values of damped response.

The phase angle is described by

$$\text{phase angle} = \cos^{-1}\left[\frac{\text{real value of stiffness}}{\{\text{real value of stiffness}\}^2 + \{\text{imaginary value of stiffness}\}^2}\right] \tag{85}$$

The normalized value of forcing frequency is plotted by multiplying the constant value of $\sqrt{\frac{\rho L^2}{G_{12}}}$ rad/sec. The amplitude and phase angle of the response of a viscoelastic damped system at resonance is dependent on the damping coefficient of the system (Capsoni et al., 2013). In a viscoelastic damped system, resonance occurs when damped forcing frequency is equal to undamped natural frequency (Foley et al., 2008). So, for ratio of damped forcing frequency to undamped natural frequency much lesser than 1, resonance is very close to undamped natural frequency and hence the phase difference angle is, $-\pi/2$. Also, it is noteworthy that the phase before resonance is very close to zero and after resonance is, $-\pi$ (Luongo and Zulli, 2020). Similarly, the amplitude is very low expect near the resonant frequency. When the phase angle reaches close to zero degree, then the amplitude reaches close to 1, i.e. very less amplification is observed (Joris and Yin, 1992). So, to summarize, as damping increases in the system, both the phase angle and amplitude at resonance decreases. Also, the rate of change near the neighborhood decreases which means that the transition near the resonance is smoother (Baer et al., 1989). Phase response at resonance frequency for stiffness element, $[K_{33}]$ and $[K_{66}]$ of FRCP is changing from one phase to another phase. The phase propagation through the composite panel has negative and positive slope at the left and right side of the resonance frequency, respectively. So, the medium has a band-gap region of zero wave propagation at resonance, which results in constant phase across the medium (Aydin et al., 2004). In other words, the propagation of the wave is backward at the resonance which results in negative phase slope across the medium (Nguyen et al., 2018).

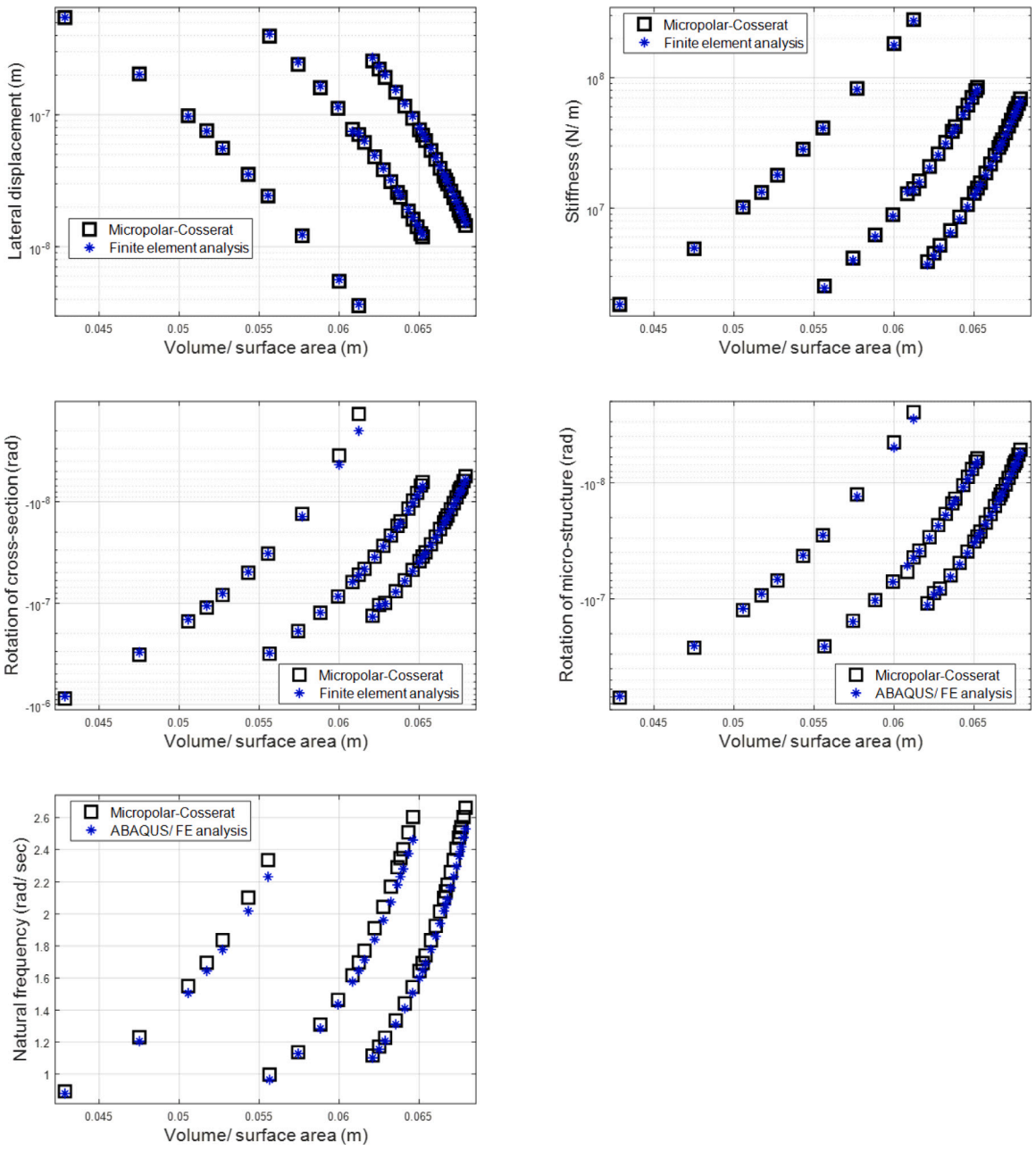

Fig. 5. In-plane static and dynamic response of undamped transversely isotropic layered composite panel. Natural frequency is scaled by a proper factor, $\sqrt{\frac{\rho L^2}{G_{12}}}$.

7. Summary of the results

One-dimensional Micropolar-Cosserat anisotropic elastic beam theory is used to evaluate the in-plane damped and undamped response of the composite panel. The conclusion from the study of static and dynamic systems are listed below.

7.1. Damped systems

- The analytical expression is derived for the external as well as internal damping system. The dynamic response shown in the plots is limited to the internal damping.
- The analytical response of internal damping is evaluated by spectral element method within state space framework.
- Mathematical response and significance of damped FRCP, displacement, diagonal stiffness and phase angle are presented.
- In-plane static response and natural frequency show good agreement for undamped response, as depicted in Fig. 6

7.2. Undamped systems

7.2.1. Static systems

- This system is able to predict the presence of curvature or micro-rotational displacement field of fiber deformation.
- Spectral element method within state–space framework is used for the snapshot of macro and micro displacements of composite panels.
- Finite element model of panel is validated with Micropolar-Cosserat analysis.
- The comparative study shows that difference in macro and micro-deflection, and stiffness are less than 3%; when the width of infill walls is limited up to $0.75L$.

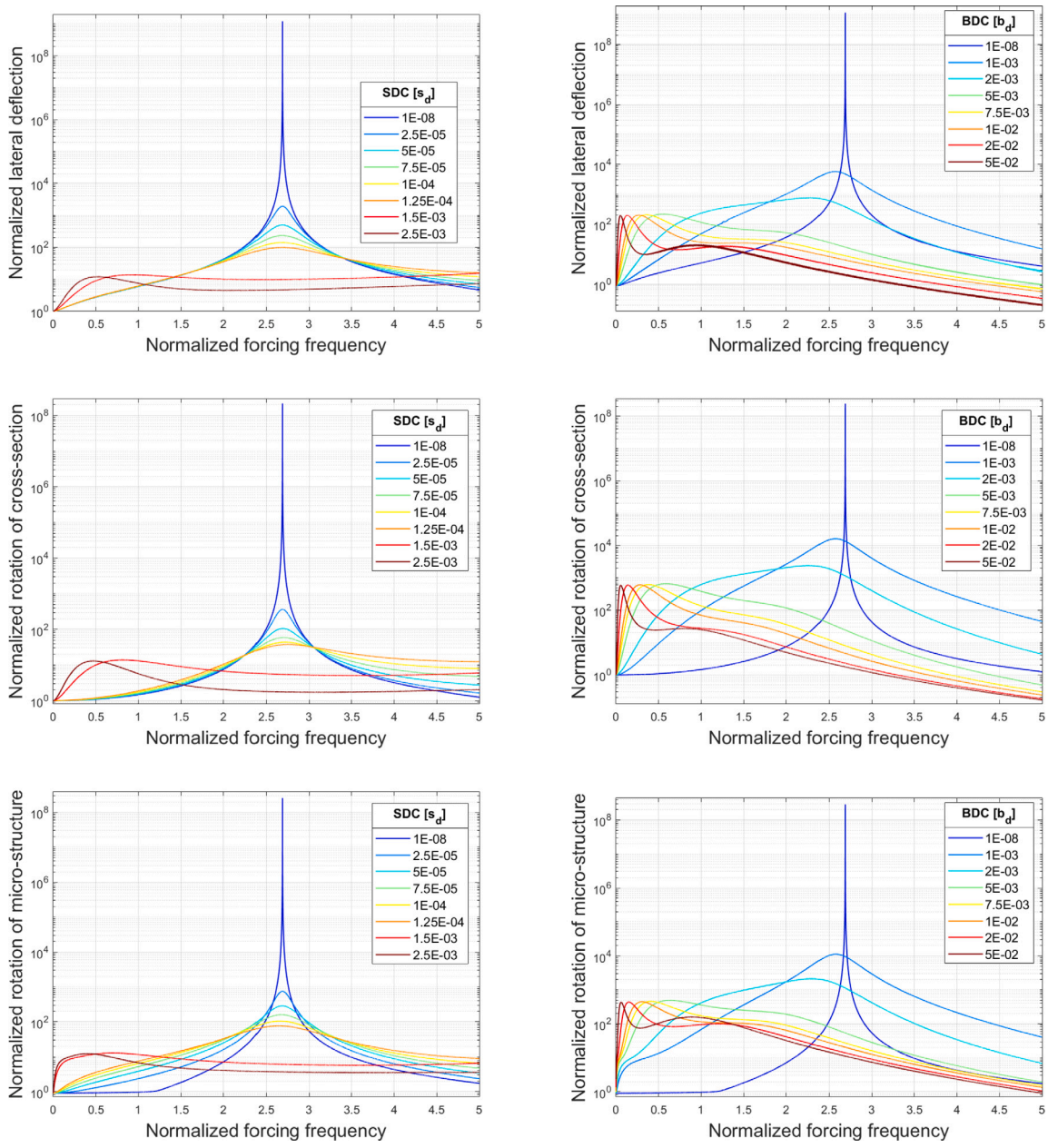

Fig. 6. Variation of coefficient of bending stress, b_d and shear stress, s_d for the composite panel; size of panel 1 m × 1 m × 0.15 m.

7.2.2. Dynamic systems

- The Micropolar-Cosserat FRCP is able to predict the presence of the dispersive phenomenon of flexural waves.
- Spectral element method is used for evaluating the natural frequencies of panels.
- Finite element simulations of panel walls and Micropolar-Cosserat theory shows good agreement.
- The comparative study shows that difference in natural frequencies are less than 5%; when the width of infill walls is limited up to $0.75L$.

8. Conclusions

The micromechanics of lamina's approach for homogenized fiber–matrix structure is very advantageous in predicting the behavior of the composites, accurately. But, asymmetric curvature pattern is observed in the FRCP due to structurally unbalanced and asymmetrical orientation of lamina about the mid-plane. The ESL theory into Micropolar-Cosserat continuum provides a good agreement to macro and micro-deformation, and natural frequency using the spectral element method; when compared with plane stress FE model. The contribution of the paper and novelty of this work includes:

- The micro-mechanical conversion of local to global lamina based on Rodrigues' rotational formula for damped composite panel is the unique features of this study.
- The proposed analytical approach using spectral element method with in state–space framework can be used to evaluate the damped response of composite panel for any type of boundary conditions.
- In the present paper, the curvature force has been considered due to asymmetric shear at free end to find the exact undamped and damped response of FRCP.

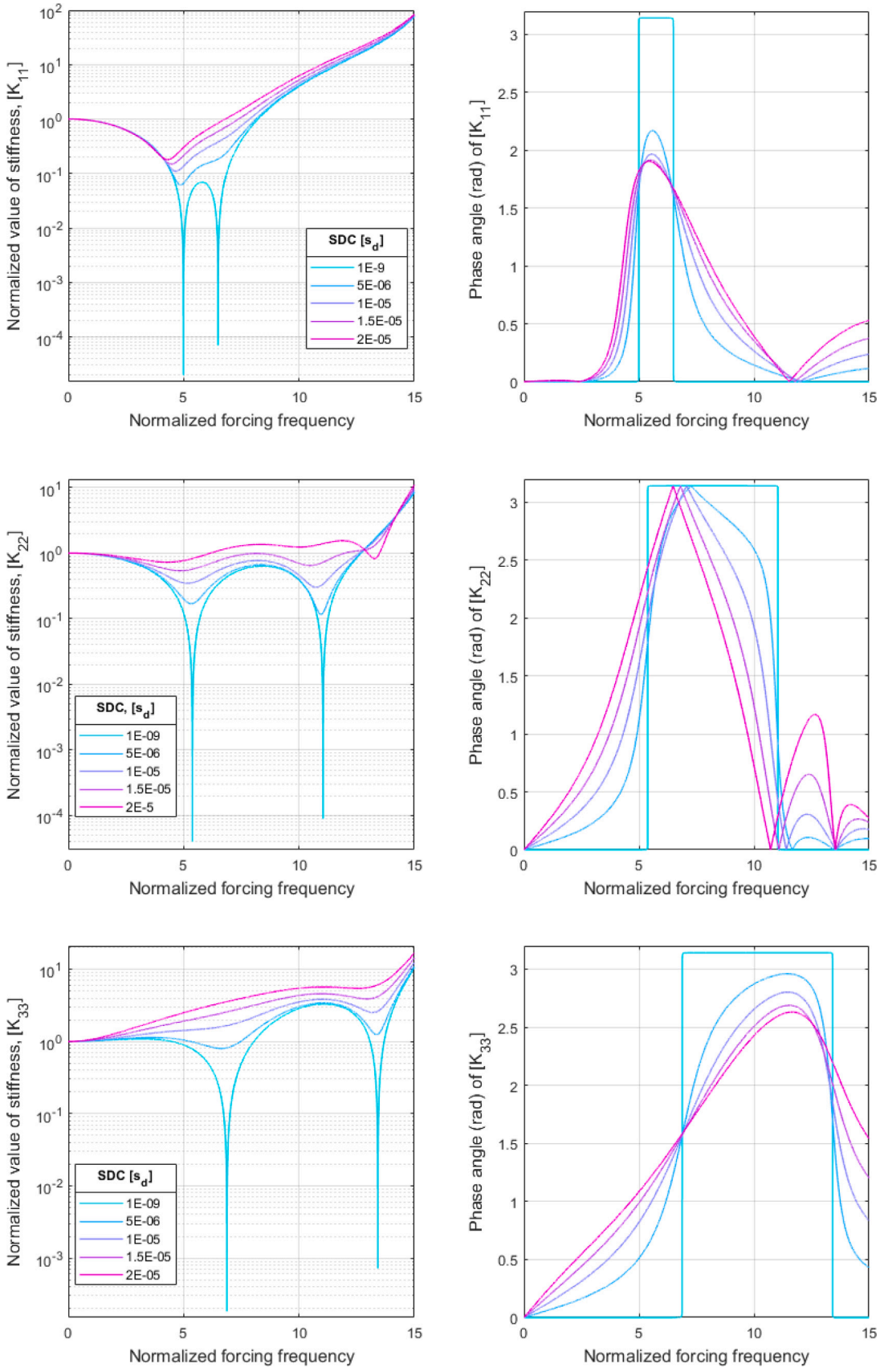

Fig. 7. Variation of coefficient of bending stress, s_d for the elements of diagonal stiffness matrix of panel; size of panel 1 m × 1 m × 0.15 m.

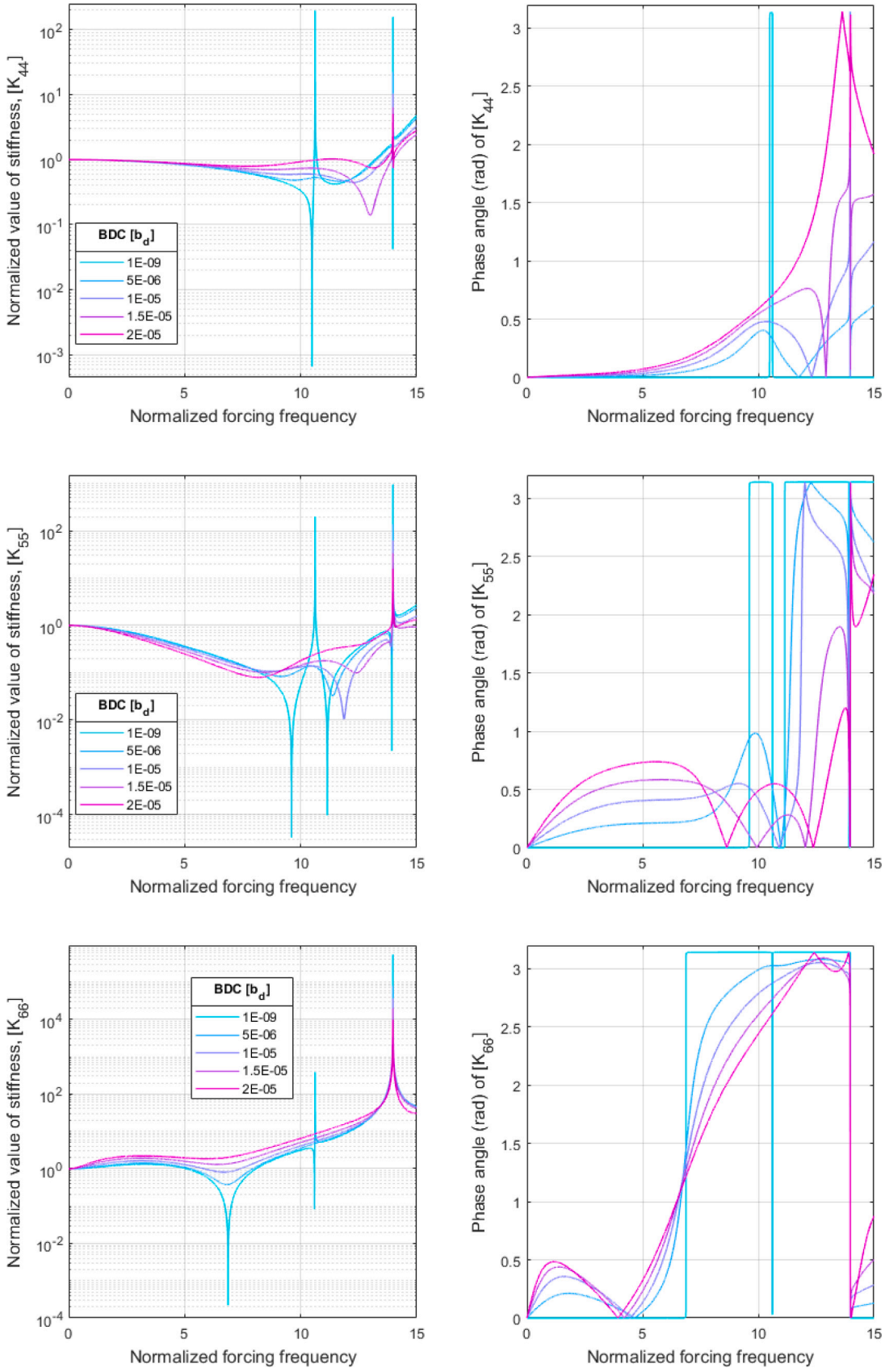

Fig. 8. Variation of coefficient of shear stress, b_d for the elements of diagonal stiffness matrix of panel; size of panel 1 m × 1 m × 0.15 m.

- The validation of theoretical independent micro-rotation of panel with the help of undamped static response of the plane-stress element has not been presented before elsewhere.
- The analytical results evidenced a good agreement with finite element analysis due to incorporation of proposed exact boundary condition at free end.

On the basis of the study of transversely isotropic Micropolar-Cosserat layered composite panels conducted here, future works will consider damping evaluation of composite panels with auxetic core material. This will help to customize overall damping in composite materials.

Declaration of competing interest

The authors declare that they have no known competing financial interests or personal relationships that could have appeared to influence the work reported in this paper.

Acknowledgments

AB acknowledges Inspire faculty awards, Department of Science and Technology, (DST grant): DST/INSPIRE /04/2018/000052. SKS, AB, and RV acknowledge Indo-Canada (IC Impact grant): DST/INT/CAN/P-03/2019 for partial financial support.

Appendix. Elastic stiffness composite panel

A.1. Fiber properties of lamina

$E_{11} = E_f V_f + E_m V_m$, $E_{22} = \frac{E_f E_m}{E_f V_m + E_m V_f}$, $G_f = \frac{E_f}{2(1+\nu_f)}$, $G_m = \frac{E_m}{2(1+\nu_m)}$, $G_{12} = \frac{G_f G_m}{G_f V_m + G_m V_f}$, $\nu_{12} = \nu_f V_f + \nu_m V_m$, $\nu_{21} = \frac{\nu_{12} E_{22}}{E_{11}}$ and $\rho = \rho_f V_f + \rho_m V_m$.

where ν_f, ν_m, E_f, E_m, G_f, G_m, ρ_f, ρ_m, and $l(= 0.02 \times L)$ (Rahaman et al., 2015) are Poisson ratio, young modulus, shear modulus, density and characteristics length, for the unidirectional fiber and matrix of anisotropic domain lamina, respectively.

A.2. Constant of local constitutive matrix

$C_{11} = \frac{E_{11}^2 (\nu_{23} - 1)}{\Delta}$, $C_{22} = \frac{E_{22}(E_{22}\nu_{12}^2 - E_{11})}{\Delta(1+\nu_{23})}$, $C_{12} = C_{21} = \frac{E_{11}E_{22}\nu_{12}}{\Delta}$, $C_{33} = G_{12}, C_{34} = \frac{G_{12}}{27}, C_{44} = \frac{G_{12}}{9}, C_{55} = 2G_{12}l^2$, $\Delta = 2E_{22}\nu_{12}^2 + E_{11}(\nu_{23} - 1)$, $D_{1111} = C_{11}$, $D_{2222} = C_{22}$, $D_{1122} = C_{12}$, $D_{1212} = C_{33} + \frac{1}{4}C_{44} + 2C_{34}$, $D_{1221} = C_{33} - \frac{1}{4}C_{44}$, $D_{2121} = C_{33} + \frac{1}{4}C_{44} - 2C_{34}$, $D_{1313} = C_{55}$, and $D_{2323} = C_{66}$ (Rahaman et al., 2015; Hasanyan and Waas, 2018b).

A.3. Constant of global constitutive matrix

A.3.1. Damped system

$A_{1111_{\xi i}} = C_{11}\frac{M_{cs}\xi_\sigma}{P_{cs}} + 2C_{33}\frac{s^2\xi_\tau}{P_{cs}}, A_{1112_{\xi i}} = C_{11}\frac{sM_{cs}\xi_\sigma}{cP_{cs}} - C_{33}\frac{sM_{cs}\xi_\tau}{cP_{cs}}$, $A_{1121_{\xi i}} = -C_{34}\frac{s\xi_\tau}{cP_{cs}}$, $A_{1211_{\xi i}} = 2C_{11}\frac{cs\xi_\sigma}{P_{cs}} - 2C_{33}\frac{cs\xi_\tau}{P_{cs}}$, $A_{1212_{\xi i}} = 2C_{11}\frac{s^2\xi_\sigma}{P_{cs}} + C_{33}\frac{M_{cs}\xi_\tau}{P_{cs}}$, $A_{1221_{\xi i}} = \frac{C_{34}\xi_\tau}{P_{cs}}$, $A_{2111_{\xi i}} = -2cs\xi_\tau C_{34}$, $A_{2112_{\xi i}} = C_{34}M_{cs}\xi_\tau$, $A_{2121_{\xi i}} = \xi_\tau C_{44}$, $D_{11_{\xi i}} = \xi_m C_{55}$, $M_{cs} = c^2 - s^2$, and $P_{cs} = c^2 + s^2$.

A.3.2. Undamped system

$A_{1111_i} = C_{11}\frac{M_{cs}}{P_{cs}} + 2C_{33}\frac{s^2}{P_{cs}}, A_{1112_i} = C_{11}\frac{sM_{cs}}{cP_{cs}} - C_{33}\frac{sM_{cs}}{cP_{cs}}, A_{1121_i} = -C_{34}\frac{s}{cP_{cs}}$, $A_{1211_i} = 2C_{11}\frac{cs}{P_{cs}} - 2C_{33}\frac{cs}{P_{cs}}, A_{1212_i} = 2C_{11}\frac{s^2}{P_{cs}} + C_{33}\frac{M_{cs}}{P_{cs}}$, $A_{1221_i} = \frac{C_{34}}{P_{cs}}$, $A_{2111_i} = -2csC_{34}$, $A_{2112_i} = C_{34}M_{cs}$, $A_{2121_i} = C_{44}$, $D_{11} = C_{55}$, $M_{cs} = c^2 - s^2$, and $P_{cs} = c^2 + s^2$.

A.4. Stiffness parameter of ESL

A.4.1. Damped system

$B_{11_{\xi i}} = \left(A_{1212_{\xi i}} - A_{2112_{\xi i}}\right)$, $B_{12_{\xi i}} = \left(A_{1221_{\xi i}} - A_{2121_{\xi i}}\right)$, $B_{21_{\xi i}} = \left(A_{1212_{\xi i}} + A_{2112_{\xi i}}\right)$, $B_{22_{\xi i}} = \xi i\left(A_{1221_{\xi i}} + A_{2121_{\xi i}}\right)$, $E_{11_{\xi i}} = \left(B_{11_{\xi i}} + B_{12_{\xi i}}\right)$, $E_{12_{\xi i}} = \left(B_{11_{\xi i}} - B_{12_{\xi i}}\right)$, $E_{21_{\xi i}} = \left(B_{21_{\xi i}} + B_{22_{\xi i}}\right)$, and $E_{22_{\xi i}} = \left(B_{21_{\xi i}} - B_{22_{\xi i}}\right)$.

A.4.2. Undamped system

$B_{11_i} = \left(A_{1212_i} - A_{2112_i}\right)$, $B_{12_i} = \left(A_{1221_i} - A_{2121_i}\right)$, $B_{21_i} = \left(A_{1212_i} + A_{2112_i}\right)$, $B_{22_i} = \left(A_{1221_i} + A_{2121_i}\right)$, $E_{11_i} = \left(B_{11_i} + B_{12_i}\right)$, $E_{12_i} = \left(B_{11_i} - B_{12_i}\right)$, $E_{21_i} = \left(B_{21_i} + B_{22_i}\right)$, and $E_{22_i} = \left(B_{21_i} - B_{22_i}\right)$.

Where i = number of transversely isotropic lamina of having either the same or differing properties and $i = 1, 2, \ldots k$. The maximum value of k is 3.

References

Adams, R., Maheri, M., 1994. Dynamic flexural properties of anisotropic fibrous composite beams. Compos. Sci. Technol. 50 (4), 497–514.

Adams, R.D., Maheri, M., 2003. Damping in advanced polymer–matrix composites. J. Alloys Compd. 355 (1–2), 126–130.

Adhikari, S., 2000. Damping models for structural vibration, Cambridge University Engineering Department (Ph.D. thesis). Dissertation at the University of Cambridge for the Degree of Doctor of ....

Adhikari, S., 2005. Damping modelling and identification using generalized proportional damping. In: Proceedings of the 23rd International Modal Analysis Conference (IMACXXIII), Orlando, Florida, USA.

Alshibli, K.A., Alsaleh, M.I., Voyiadjis, G.Z., 2006. Modelling strain localization in granular materials using micropolar theory: Numerical implementation and verification. Int. J. Numer. Anal. Methods Geomech. 30 (15), 1525–1544.

Anand, L., Gu, C., 2000. Granular materials: constitutive equations and strain localization. J. Mech. Phys. Solids 48 (8), 1701–1733.

Asghari, M., Kahrobaiyan, M., Rahaeifard, M., Ahmadian, M., 2011. Investigation of the size effects in Timoshenko beams based on the couple stress theory. Arch. Appl. Mech. 81 (7), 863–874.

Aydin, K., Guven, K., Katsarakis, N., Soukoulis, C.M., Ozbay, E., 2004. Effect of disorder on magnetic resonance band gap of split-ring resonator structures. Opt. Express 12 (24), 5896–5901.

Baer, S.M., Erneux, T., Rinzel, J., 1989. The slow passage through a Hopf bifurcation: delay, memory effects, and resonance. SIAM J. Appl. Math. 49 (1), 55–71.

Banerjee, A., 2020. Non-dimensional analysis of the elastic beam having periodic linear spring mass resonators. Meccanica 1–11.

Banks, H.T., Inman, D., 1991. On damping mechanisms in beams.

Bardet, J., 1994. Observations on the effects of particle rotations on the failure of idealized granular materials. Mech. Mater. 18 (2), 159–182.

Benayoune, A., Samad, A.A., Trikha, D., Ali, A.A., Ellinna, S., 2008. Flexural behaviour of pre-cast concrete sandwich composite panel–experimental and theoretical investigations. Constr. Build. Mater. 22 (4), 580–592.

Capsoni, A., Viganò, G.M., Bani-Hani, K., 2013. On damping effects in Timoshenko beams. Int. J. Mech. Sci. 73, 27–39.

Carrera, E., Zozulya, V., 2020a. Carrera unified formulation (CUF) for the micropolar plates and shells. I. Higher order theory. Mech. Adv. Mater. Struct. 1–23.

Carrera, E., Zozulya, V., 2020b. Carrera unified formulation (CUF) for the micropolar plates and shells. II. Complete linear expansion case. Mech. Adv. Mater. Struct. 1–20.

Chandra, R., Singh, S., Gupta, K., 1999. Damping studies in fiber-reinforced composites–a review. Compos. Struct. 46 (1), 41–51.

Chang, C.S., Ma, L., 1991. A micromechanical-based micropolar theory for deformation of granular solids. Int. J. Solids Struct. 28 (1), 67–86.

Chau, K.T., 2017. Theory of Differential Equations in Engineering and Mechanics. CRC Press; Taylor and Francis Group.

Crane, R.M., Gillespie Jr, J.W., 1989. Damping Loss Factor Determination of Glass and Graphite Fiber Composites. Tech. rep., David Taylor Research Center Bethesda MD Ship Materials Engineering Dept.

Daniel, I.M., Ishai, O., Daniel, I.M., Daniel, I., 1994. Engineering Mechanics of Composite Materials, Vol. 3. Oxford university press New York.

Davis, A., 2014. The Characterisation and Assessment of Curvature in Asymmetric Carbon Fibre Composite Laminates (Ph.D. thesis). University of Birmingham.

De Borst, R., 1991. Simulation of strain localization: a reappraisal of the cosserat continuum. Eng. Comput..

De Borst, R., Sluys, L., 1991. Localisation in a cosserat continuum under static and dynamic loading conditions. Comput. Methods Appl. Mech. Engrg. 90 (1–3).

De Silva, C.W., 2007. Vibration Damping, Control, and Design. CRC Press.

Diana, V., Casolo, S., 2019. A full orthotropic micropolar peridynamic formulation for linearly elastic solids. Int. J. Mech. Sci. 160, 140–155.
Dion, J., Commault, C., 1993. Feedback decoupling of structured systems. IEEE Trans. Automat. Control 38 (7), 1132–1135.
Eaton, N., Drew, R., Geiger, H., 1995. Finite element stress and strain analysis in composites with embedded optical fiber sensors. Smart Mater. Struct. 4 (2), 113.
Faggiani, A., Falzon, B., 2010. Predicting low-velocity impact damage on a stiffened composite panel. Composites A 41 (6), 737–749.
Federico, S., Grillo, A., 2012. Elasticity and permeability of porous fibre-reinforced materials under large deformations. Mech. Mater. 44, 58–71.
Fleck, N.A., Shu, J.Y., 1995. Microbuckle initiation in fibre composites: a finite element study. J. Mech. Phys. Solids 43 (12), 1887–1918.
Foley, A., Howe, M., Brungart, T., 2008. Sound generated by a jet-excited spherical cavity. J. Sound Vib. 315 (1–2), 88–99.
Gay, D., 2014. Composite Materials: Design and Applications. CRC press.
Ghugal, Y., Shimpi, R., 2001. A review of refined shear deformation theories for isotropic and anisotropic laminated beams. J. Reinf. Plast. Compos. 20 (3), 255–272.
Gupta, V., Adhikari, S., Bhattacharya, B., 2020. Exploring the dynamics of hourglass shaped lattice metastructures. Sci. Rep. 10 (1), 1–12.
Hasanyan, A.D., Waas, A.M., 2018a. Compressive failure of fiber composites: A homogenized, mesh-independent model. J. Appl. Mech. 85 (9).
Hasanyan, A., Waas, A., 2018b. Localization in anisotropic elastoplastic micropolar media: Application to fiber reinforced composites. J. Mech. Phys. Solids 121, 1–22.
Hashin, Z., 1970. Complex moduli of viscoelastic composites—I. General theory and application to particulate composites. Int. J. Solids Struct. 6 (5), 539–552.
Hassanzadeh-Aghdam, M., Mahmoodi, M., Ansari, R., 2018. Micromechanics-based characterization of mechanical properties of fuzzy fiber-reinforced composites containing carbon nanotubes. Mech. Mater. 118, 31–43.
Hibbitt, Karlsson, Sorensen, 1997. ABAQUS: Theory Manual. 2, Hibbitt, Karlsson & Sorensen.
Huang, F.-Y., Yan, B.-H., Yan, J.-L., Yang, D.-U., 2000. Bending analysis of micropolar elastic beam using a 3-D finite element method. Internat. J. Engrg. Sci. 38 (3), 275–286.
Hyer, M.W., White, S.R., 2009. Stress Analysis of Fiber-Reinforced Composite Materials. DEStech Publications, Inc.
Isanaka, B.R., Akbar, M.A., Mishra, B.P., Kushvaha, V., 2020. Free vibration analysis of thin plates: Bare versus stiffened. Eng. Res. Express 2 (1), 015014.
Joris, P.X., Yin, T.C., 1992. Responses to amplitude-modulated tones in the auditory nerve of the cat. J. Acoust. Soc. Am. 91 (1), 215–232.
Kaliske, M., Rothert, H., 1995. Damping characterization of unidirectional fibre reinforced polymer composites. Compos. Eng. 5 (5), 551–567.
Karttunen, A.T., Reddy, J., Romanoff, J., 2018. Micropolar modeling approach for periodic sandwich beams. Compos. Struct. 185, 656–664.
Kundalwal, S., Ray, M., 2012. Effective properties of a novel composite reinforced with short carbon fibers and radially aligned carbon nanotubes. Mech. Mater. 53, 47–60.
Kyriakides, S., Arseculeratne, R., Perry, E., Liechti, K., 1995. On the compressive failure of fiber reinforced composites. Int. J. Solids Struct. 32 (6–7), 689–738.
Lakes, R., 2002. High damping composite materials: effect of structural hierarchy. J. Compos. Mater. 36 (3), 287–297.
Lan, X., Liu, L., Liu, Y., Leng, J., Du, S., 2014. Post microbuckling mechanics of fibre-reinforced shape-memory polymers undergoing flexure deformation. Mech. Mater. 72, 46–60.
Lekhnitskii, S., Dill, E., 1964. Theory of Elasticity of an Anisotropic Elastic Body. Holden-day.
Luongo, A., Zulli, D., 2020. Free and forced linear dynamics of a homogeneous model for beam-like structures. Meccanica 55 (4), 907–925.
Maity, M., Kundu, S., Kumhar, R., Gupta, S., 2020. Influence of mechanical imperfection on the transference of Love-type waves in viscoelastic substrate overloaded by visco-micropolar composite structure. Eng. Comput..
Matzenmiller, A., Lubliner, J., Taylor, R., 1995. A constitutive model for anisotropic damage in fiber-composites. Mech. Mater. 20 (2), 125–152.
Matzenmiller, A., Sackman, J.L., 1994. On damage induced anisotropy for fiber composites. Int. J. Damage Mech. 3 (1), 71–86.
Mikata, Y., 2019. Linear peridynamics for isotropic and anisotropic materials. Int. J. Solids Struct. 158, 116–127.
Munian, R.K., Mahapatra, D.R., Gopalakrishnan, S., 2018. Lamb wave interaction with composite delamination. Compos. Struct. 206, 484–498.
Needleman, A., 1988. Material rate dependence and mesh sensitivity in localization problems. Comput. Methods Appl. Mech. Engrg. 67 (1), 69–85.
Nettles, A.T., 1994. Basic Mechanics of Laminated Composite Plates. NASA Reference Publication 1351, MSFC Alabama, (1994).
Nguyen, Q., Zaghloul, A.I., Weiss, S., 2018. Phase response at resonance frequency for metamaterial-insert mediums. In: 2018 United States National Committee of URSI National Radio Science Meeting (USNC-URSI NRSM). IEEE, pp. 1–2.
Oda, M., Konishi, J., Nemat-Nasser, S., 1982. Experimental micromechanical evaluation of strength of granular materials: effects of particle rolling. Mech. Mater. 1 (4), 269–283.
O'neil, P.V., 2011. Advanced Engineering Mathematics. Jones and Bartlett cengage learning.
Ongaro, F., Barbieri, E., Pugno, N., 2018. Mechanics of mutable hierarchical composite cellular materials. Mech. Mater. 124, 80–99.
Rahaman, M.M., Deepu, S., Roy, D., Reddy, J., 2015. A micropolar cohesive damage model for delamination of composites. Compos. Struct. 131, 425–432.
Ramana, B.V., 2006. Higher Engineering Mathematics. Tata McGraw-Hill Education.
Ramezani, S., Naghdabadi, R., Sohrabpour, S., 2009. Analysis of micropolar elastic beams. Eur. J. Mech. A Solids 28 (2), 202–208.
Romanoff, J., Varsta, P., Klanac, A., 2007. Stress analysis of homogenized web-core sandwich beams. Compos. Struct. 79 (3), 411–422.
Roque, C., Fidalgo, D., Ferreira, A., Reddy, J., 2013. A study of a microstructure-dependent composite laminated timoshenko beam using a modified couple stress theory and a meshless method. Compos. Struct. 96, 532–537.
Sadeghpour, E., Guo, Y., Chua, D., Shim, V.P., 2020. Micro-scale computational modeling of graphene-based nanocomposites–influence of filler-matrix interface failure. Mech. Mater. 150, 103584.
Sargsyan, S.H., 2012. General theory of micropolar elastic thin shells. Phys. Mesomech. 15 (1–2), 69–79.
Sargsyan, A., Sargsyan, S., 2016. Mathematical model of the dynamics of micropolar elastic thin beams. Free and forced vibrations. Phys. Mesomech. 19 (4), 459–465.
Scerrato, D., 2014. Eff ect of Micro-Particle Addition on Frictional Energy Dissipation and Strength of Concrete: Experiments and Modelling (Ph.D. thesis). Sapienza Università di Roma (Italie); INSA de Lyon (France).
Seidel, G.D., Lagoudas, D.C., 2006. Micromechanical analysis of the effective elastic properties of carbon nanotube reinforced composites. Mech. Mater. 38 (8–10), 884–907.
Sevostianov, I., Abaimov, S., Trofimov, A., 2018. Replacement relations for thermal conductivities of heterogeneous materials having different matrices. Mech. Mater. 121, 50–56.
Sharma, A., Kumar, S.A., Kushvaha, V., 2020. Effect of aspect ratio on dynamic fracture toughness of particulate polymer composite using artificial neural network. Eng. Fract. Mech. 228, 106907.
Sigmund, O., 1995. Tailoring materials with prescribed elastic properties. Mech. Mater. 20 (4), 351–368.
Singh, S., Banerjee, A., Varma, R., Adhikari, S., Das, S., 2021. Static and dynamic analysis of homogeneous micropolar-cosserat panels. Mech. Adv. Mater. Struct. 1–53.
Singh, A.K., Chaki, M.S., Chattopadhyay, A., 2018. Remarks on impact of irregularity on SH-type wave propagation in micropolar elastic composite structure. Int. J. Mech. Sci. 135, 325–341.
Sodano, H.A., Park, G., Inman, D.J., 2004. An investigation into the performance of macro-fiber composites for sensing and structural vibration applications. Mech. Syst. Signal Process. 18 (3), 683–697.
Steigmann, D.J., 2015. Effects of fiber bending and twisting resistance on the mechanics of fiber-reinforced elastomers. In: Nonlinear Mechanics of Soft Fibrous Materials. Springer, pp. 269–305.
Suarez, S.A., Gibson, R.F., Sun, C., Chaturvedi, S., 1986. The influence of fiber length and fiber orientation on damping and stiffness of polymer composite materials. Exp. Mech. 26 (2), 175–184.
Torvik, P.J., 2010. Material and slip damping. In: Harris' Shock and Vibraiton Handbook. pp. 932–960.
Treviso, A., Van Genechten, B., Mundo, D., Tournour, M., 2015. Damping in composite materials: Properties and models. Composites B 78, 144–152.
Wanji, C., Chen, W., Sze, K., 2012. A model of composite laminated Reddy beam based on a modified couple-stress theory. Compos. Struct. 94 (8), 2599–2609.
Yerramalli, C.S., Waas, A.M., 2004. The effect of fiber diameter on the compressive strength of composites-A 3D finite element based study. Comput. Model. Eng. Sci. 6, 1–16.
Zhou, W., Liu, D., Liu, N., 2017. Analyzing dynamic fracture process in fiber-reinforced composite materials with a peridynamic model. Eng. Fract. Mech. 178, 60–76.
Zozulya, V., 2018. Higher order theory of micropolar plates and shells. ZAMM J. Appl. Math. Mech. Zeitschrift FUR Angewandte Mathematik Und Mechanik 98 (6), 886–918.